2.17 Properties of Rocks and Minerals – Physical Origins of Anelasticity and Attenuation in Rock

I. Jackson, Australian National University, Canberra, ACT, Australia

Nomenclature

a	spacing between adjacent Peierls valleys
a_d	period of kink potential measured parallel to dislocation line
b	Burgers vector
d	grain size; characteristic separation of vacancy sources
f	frequency; the reciprocal of $du/dx = \tan\phi$ (**Figure 4(c)**)
g	dimensionless multiplier of T_m/T in exponent for thermal activation of relaxation time

h	separation of closely spaced dislocations in subgrain wall
h_j	jth coefficient in Fourier series representing grain-boundary topography
k	Boltzmann constant
m_l	effective mass per unit length of dislocation
n	exponent in term βt^n representing transient creep in the Andrade model
p	internal variable providing link between stress and anelastic strain
$p_L(L)$	distribution of dislocation segment lengths
p_s	small fluctuation in pressure P
p_0	stress-dependent equilibrium value
s	Laplace transform variable; distance measured along dislocation line; exponent describing grain-size sensitivity of Q^{-1}
t	time
u	displacement of dislocation segment, or position of grain boundary, in y-direction
u_0	x-independent amplitude of u; position of straight dislocation segment under static stress σ
u_m	maximum displacement for newly formed kink pair
w_k	width of a single geometrical kink
x	coordinate measuring distance parallel to dislocation line or grain boundary
x_1	unstable equilibrium spacing of kinks of opposite sign
y	coordinate measuring distance perpendicular to dislocation line
A	measure of anisotropy or inter-phase variability in elastic moduli or thermal expansivity involved in thermoelastic relaxation strength
B	dislocation drag coefficient
C_{OH}	concentration of hydroxyl ions
D	diffusivity (either of matter or heat)
$D(\tau)$	normalised distribution of anelastic relaxation times
D_b	grain-boundary diffusivity
D_k	kink diffusivity
D_{mc}	multicomponent diffusivity
E	activation energy for relaxation time
E_d	elastic strain energy per unit length of dislocation or line tension
E_P	activation energy describing position (period) of dissipation peak
E_{up}	binding energy of dislocation to pinning point
G	shear modulus
G_m	free energy of kink migration
G_{HS}	mean of the Hashin–Shtrikmann bounds on the shear modulus of a polycrystalline aggregate
G_R	relaxed value of shear modulus (anelastic relaxation only)
G_{RS}	Reuss average of single-crystal elastic constants for shear
G_U	unrelaxed shear modulus
H_{int}	kink interaction energy
H_k	formation energy for a single geometrical kink
H_{kp}	kink-pair formation energy
H_m	enthalpy of kink migration
H_{mc}	activation enthalpy for multicomponent diffusion
$J(t)$	creep function
J_1	real part of J^*
J_2	negative imaginary part of J^*
J_U	unrelaxed compliance (ε/σ)
J^*	dynamic compliance
K_f	bulk modulus of fluid
K_m	bulk modulus of melt
K_s	bulk modulus of solid matrix
$\underline{K}$	bulk modulus of composite of coexisting phases
L	length of dislocation segment between adjacent pinning points
L_c	critical dislocation segment length for dislocation multiplication
$\underline{L}$	subgrain diameter
N	number of terms retained in Fourier series representing grain-boundary topography
N_v	number of dislocation segments of given length L per unit volume
P	of internal variable p
Q^{-1}	inverse quality factor ($=\tan\delta$), a measure of strain energy dissipation
Q_D^{-1}	height of the Debye dissipation peak of the standard anelastic solid
R	radius of curvature of dislocation bowed out under applied stress; gas constant; radius of grain-edge tubule

S_m	entropy of kink migration
T	absolute temperature
T_m	melting temperature
T_o	oscillation period ($=2\pi/\omega$)
U	equilibrium distance for grain-boundary sliding
$U(u)$	Peierls potential
X	chemical composition
Y	Youngs modulus
α	negative of exponent describing frequency dependence of Q^{-1}
α_b	aspect ratio of grain-boundary region ($=\delta$/d)
α_e	aspect ratio (minimum/maximum dimension) of ellipsoidal inclusion
α_t	aspect ratio of grain-edge tubule ($=2$R/d)
β	coefficient of term βt^n representing transient creep in the Andrade model
γ	multiplicative constant of order unity
γ_s	multiplicative constant
δ	phase lag between stress and strain; width of grain-boundary region ($<<d$)
δG	anelastic relaxation of the shear modulus
δJ	anelastic relaxation of the compliance
δP	width in pressure of binary loop
δT_0	width of melting interval
δT_s	pressure-induced perturbation to solidus and liquidus temperatures
$\delta\phi$	pressure-induced perturbation in melt fraction
ε	strain
ε_a	anelastic strain
ε_e	elastic strain
ε_m	maximum anelastic strain due to migration of geometrical kinks on a dislocation segment
ε_0	amplitude of sinusoidally time-varying strain
η	viscosity or effective viscosity
η_1	viscosity of dashpot in parallel with spring in the anelastic element of the Burgers model
η_b	grain-boundary viscosity
η_f	fluid viscosity
η_m	melt viscosity
λ	wavelength of periodic grain-boundary topography or of seismic wave
μ_k	kink mobility ($=D_k/kT$)
ν	Poisson's ratio
ν_{k0}	attempt frequency of dislocation vibration
ρ	crystal density
ρ_k^-, ρ_k^+	densities of kinks of opposite sign (number per unit length of dislocation line)
ρ_{k0}^-, ρ_{k0}^+	as above, under conditions of zero stress
ρ_k^{eq}	equilibrium kink density: number of kinks per unit length of dislocation line
σ	stress, usually shear stress
σ_n	normal stress
σ_P	Peierls stress
σ_t	tectonic shear stress
σ_{up}	unpinning shear stress
σ_0	amplitude of sinusoidally time-varying stress
τ	relaxation time
τ_A	anelastic relaxation time
τ_d	duration of transient diffusional creep
τ_{dr}	timescale for draining of cylindrical laboratory specimen
τ_e	relaxation time for elastically accommodated grain-boundary sliding
τ_M	Maxwell (viscous) relaxation time
$\tau_{s,t}$	relaxation time for melt squirt between grain-edge tubules
$\tau_{s,e}$	relaxation time for melt squirt between ellipsoidal inclusions
ϕ	melt fraction; the angle betweeen a dislocation segment and its Peierls valley
ω	angular frequency
ω_0	(angular) resonance frequency of dislocation segment
Γ	Gamma function
Δ	anelastic relaxation strength
Λ	dislocation density, that is, dislocation length per unit volume $=N_vL$
Λ_m	density of mobile dislocations
Ω	molecular volume of diffusing species
$(\delta\rho/\rho)_0$	fractional density contrast between coexisting polymorphs
$(\delta\rho/\rho)_a$	fractional change in density resulting from small change in proportions of coexisting phases; anelastic volumetric strain
$(\delta\rho/\rho)_e$	fractional change in density caused by pressure p_s

2.17.1 Introduction

The Earth and its constituent materials are subjected to naturally applied stresses that vary widely in intensity and timescale. At sufficiently high temperatures, nonelastic behavior will be encountered – even at the low stress amplitudes of seismic wave propagation, tidal forcing, and glacial loading (**Figure 1**). For harmonic loading, nonelastic behavior is manifest in a phase lag between stress and strain giving rise to strain energy dissipation and associated frequency dependence (dispersion) of the relevant modulus or wave speed. In the case of glacial loading, the transient creep of mantle material of sufficiently low viscosity allows time-dependent relaxation of the stresses imposed by the growth and decay of ice sheets with consequent time-dependent surface deformations.

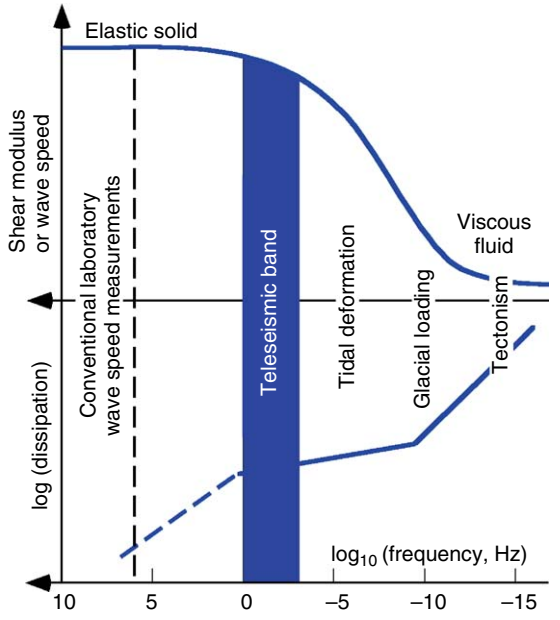

Figure 1 A schematic mechanical relaxation spectrum for the Earth. The mechanical behavior of the Earth's hot interior and its constituent materials change progressively from that of an elastic solid to that of a viscous fluid with decreasing frequency or increasing timescale. This transition involves the thermally activated mobility of crystal defects including vacancies, dislocations, twin domain and grain boundaries, and of phase boundaries and intergranular melt. The resulting viscoelastic behavior is manifest in the dissipation of strain energy and associated frequency dependence of the shear modulus and wavespeed. Adapted from Jackson I, Webb SL, Weston L, and Boness D (2005) Frequency dependence of elastic wave speeds at high-temperature: A direct experimental demonstration. *Physics of the Earth and Planetary Interiors* 148: 85–96.

Departures from elastic behavior have long been studied in metals. Notable early successes came from the application of resonance (pendulum) methods at fixed frequencies near 1 Hz that revealed low-temperature dissipation peaks attributable to various types of point-defect relaxation (e.g., Zener, 1952; Nowick and Berry, 1972). Until recently most of the available information concerning elastic wave speeds in geological materials and their variations with pressure and temperature came from ultrasonic and opto-acoustic techniques at frequencies at least six orders of magnitude higher than those of teleseismic waves (**Figure 1**). However, there is growing recognition of the need for a thorough understanding of viscoelastic behavior in minerals and rocks at low strains and seismic frequencies. It is the purpose of this article to assess the relaxation mechanisms most likely to produce significant departures from elastic behavior under the high-temperature conditions of the Earth's interior. Among these are intragranular mechanisms involving the motion of point defects and dislocations, grain-boundary migration and sliding, the stress-induced redistribution of an intergranular fluid phase, and effects associated with phase transformations.

Section 2.17.2 focuses on the theoretical framework for the description of viscoelasticity provided by broad phenomenological considerations and models for the operation of specific microphysical relaxation mechanisms. A thorough review of this material in a materials science context is provided by Schaller *et al.* (2001). In Section 2.17.3, an attempt will be made to integrate the results of the still relatively few seismic-frequency laboratory experiments on geological materials into the theoretical framework. Section 2.17.4 outlines selected applications of the emerging understanding of viscoelastic relaxation in the interpretation of seismological wave speed and attenuation models.

2.17.2 Theoretical Background

2.17.2.1 Phenomenological Description of Viscoelasticity

For sufficiently small stresses, the stress–strain behavior is expected to be linear and the response is represented in the time domain by the 'creep function' $\mathcal{J}(t)$ which is defined as the strain resulting from the application at time $t = 0$ of unit step-function stress, that is,

$$\begin{aligned} \sigma(t) &= 0, \quad t < 0 \\ &= 1, \quad t \geq 0 \end{aligned} \qquad [1]$$

(e.g., Nowick and Berry, 1972). For the special case of elastic behavior, the strain appears essentially instantaneously (delayed only by the finiteness of the elastic wave speeds), and thereafter remains constant for the duration of stress application. However, at high temperatures and low frequencies, the response $\mathcal{J}(t)$ will usually be more complicated than the elastic ideal, involving in addition to the instantaneous (elastic) component, a time-dependent contribution which may be a mixture of recoverable (anelastic) and irrecoverable (viscous) strains (**Figure 2**). The simplest moderately realistic example of such linear viscoelastic rheology, that can be constructed from (elastic) springs and (viscous) dashpots arranged in series and parallel combinations, is the Burgers model (e.g., Findley *et al.*, 1976; Cooper, 2003) with the creep function

$$\mathcal{J}(t) = \mathcal{J}_U + \delta\mathcal{J}\,[1 - \exp(-t/\tau)] + t/\eta \qquad [2]$$

$\mathcal{J}_U$ and $\delta\mathcal{J}$ are the magnitudes of the instantaneous (elastic) and anelastic (time-dependent but recoverable) contributions, whereas τ and η are the time constant for the development of the anelastic response, and the steady-state Newtonian viscosity, respectively (**Figure 2**). The widely used 'standard anelastic solid' (e.g., Nowick and Berry, 1972) is the Burgers model without the series dashpot; its creep function is accordingly given by the first two terms of eqn [2]. More empirically successful in the description of transient creep, but physically less transparent, is the Andrade model (e.g., Poirier, 1985) for which the creep function is

$$\mathcal{J}(t) = \mathcal{J}_U + \beta t^n + t/\eta, \quad 1/3 < n < 1/2 \qquad [3]$$

The middle term with coefficient β and time t raised to the fractional power n represents transient creep. The relative merits of these alternative models as parametrizations of the high-temperature torsional microcreep behavior of our experimental assemblies have recently been evaluated. It has been found that the βt^n term in the Andrade model typically better fits the early part of a torsional microcreep record than does the Burgers model with its unique anelastic relaxation time τ. However, the Burgers model, generalized to include a suitable distribution $D(\tau)$ of relaxation times,

$$\mathcal{J}(t) = \mathcal{J}_U\left\{1 + \Delta\int_0^\infty D(\tau)[1 - \exp(-t/\tau)]\,d\tau\right\} + t/\eta \qquad [4]$$

provides a versatile alternative to the Andrade model in describing the viscoelastic rheology revealed, for example, by experimental torsional microcreep tests. In eqn [4], Δ is the fractional increase in compliance associated with complete ($t = \infty$) anelastic relaxation, known as the relaxation strength.

The strain $\varepsilon(t) = \varepsilon_0 \exp i(\omega t - \delta)$ resulting from the application of sinusoidally time-varying stress $\sigma(t) = \sigma_0 \exp(i\omega t)$, can be evaluated from the creep function provided that the behavior is linear (i.e., described by a differential equation which is linear in stress and strain and their respective time derivatives). This is done by superposition of the responses to each of a series of infinitesimal step-function applications of stress, that together represent the history $\sigma(t)$ of stress application (e.g., Nowick and Berry, 1972). Thus, an expression is obtained for the 'dynamic compliance' $\mathcal{J}^*(\omega)$ given by

$$\mathcal{J}^*(\omega) = \varepsilon(t)/\sigma(t) = i\omega\int_0^\infty \mathcal{J}(\xi)\exp(-i\omega\xi)\,d\xi \qquad [5]$$

where $\omega = 2\pi f$ is the angular frequency. This integral is the Laplace transform of $\mathcal{J}(t)$ with transform variable $s = i\omega$, or equivalently, within a multiplicative constant, the Fourier transform of the function which is $\mathcal{J}(\xi)$ for $\xi \geq 0$ and zero elsewhere. Since the Laplace transforms of each of the terms in the Burgers and Andrade creep functions are tabulated in standard compilations (e.g., Abramowitz and Stegun, 1972), analytical expressions for the dynamic compliance are readily derived (e.g., Jackson, 2000).

Thus, the dynamic compliance $\mathcal{J}^*(\omega)$ for the simple Burgers model is

$$\mathcal{J}^*(\omega) = \mathcal{J}_U + \delta\mathcal{J}/(1 + i\omega\tau) - i/\eta\omega \qquad [6]$$

with real and negative imaginary parts

$$\begin{aligned}\mathcal{J}_1(\omega) &= \mathcal{J}_U + \delta\mathcal{J}/(1 + \omega^2\tau^2)\\ \mathcal{J}_2(\omega) &= \omega\tau\delta\mathcal{J}/(1 + \omega^2\tau^2) + 1/\eta\omega\end{aligned} \qquad [7]$$

For the generalized Burgers model the equivalent expressions are

$$\begin{aligned}\mathcal{J}^*(\omega) &= \mathcal{J}_U\left\{1 + \Delta\int_0^\infty D(\tau)\,d\tau/(1 + i\omega\tau)\right\} - i/\eta\omega\\ \mathcal{J}_1(\omega) &= \mathcal{J}_U\left\{1 + \Delta\int_0^\infty D(\tau)\,d\tau/(1 + \omega^2\tau^2)\right\}\\ \mathcal{J}_2(\omega) &= \omega\mathcal{J}_U\,\Delta\int_0^\infty \tau D(\tau)\,d\tau/(1 + \omega^2\tau^2) + 1/\eta\omega\end{aligned} \qquad [8]$$

For the Andrade model, the corresponding expressions are

$$\begin{aligned}\mathcal{J}^*(\omega) &= \mathcal{J}_U + \beta\Gamma(1 + n)(i\omega)^{-n} - i/\eta\omega\\ \mathcal{J}_1(\omega) &= \mathcal{J}_U + \beta\Gamma(1 + n)\omega^{-n}\cos(n\pi/2)\\ \mathcal{J}_2(\omega) &= \beta\Gamma(1 + n)\omega^{-n}\sin(n\pi/2) + 1/\eta\omega\end{aligned} \qquad [9]$$

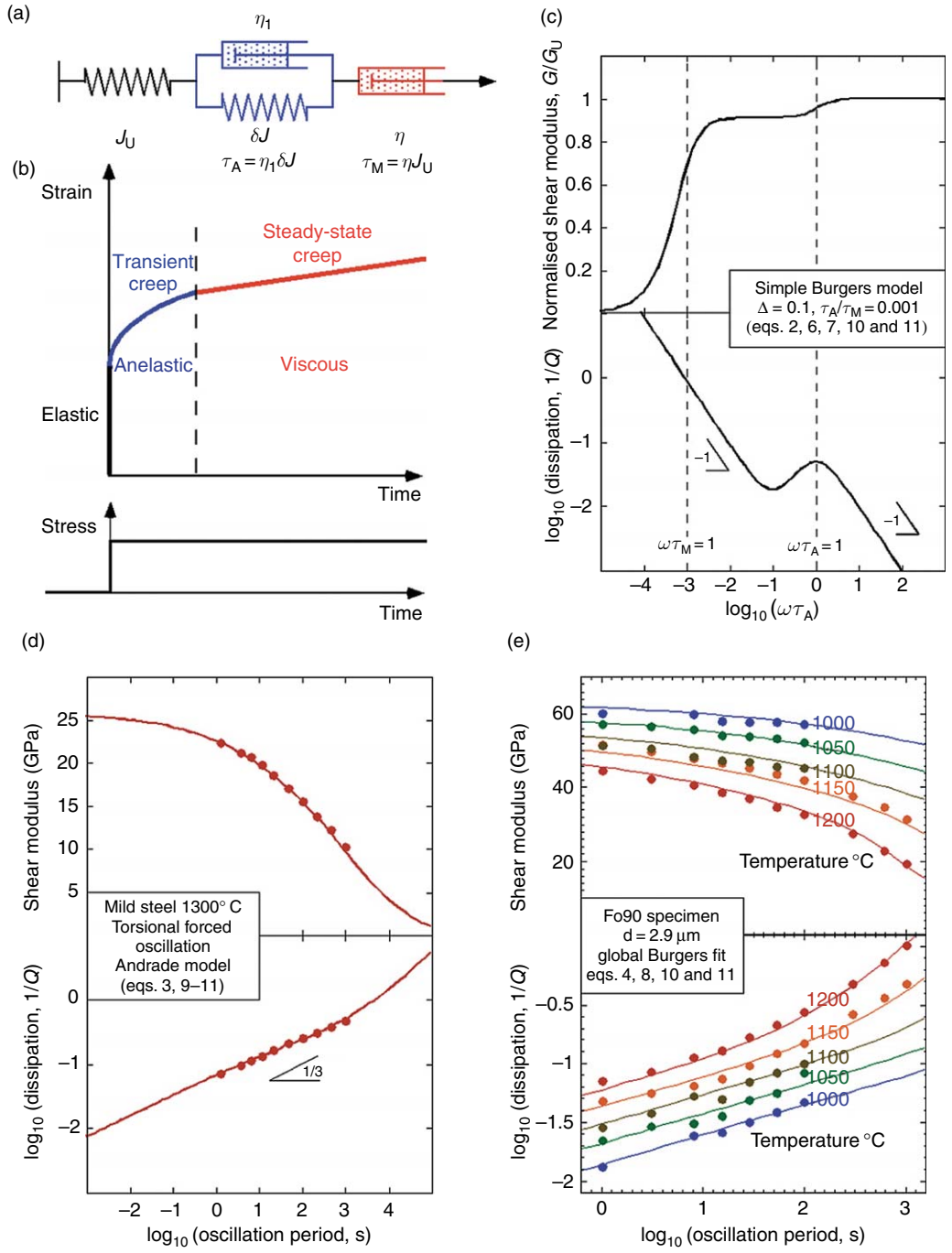

Figure 2 The Burgers and Andrade models for viscoelastic behavior. (a) Construction of the Burgers model from series and parallel combinations of Hookean springs and linear viscous dashpots. (b) The creep function for the Burgers model (eqn [2]). (c) The frequency-dependent shear modulus and dissipation for the Burgers model with $\Delta = 0.1$ and $\tau_M/\tau_A = 10^3$ (eqns [7], [10], and [11]). (d) The variations of shear modulus and dissipation for the Andrade model. The broad absorption band, within which $Q^{-1} \sim T_o^n$ (or ω^{-n}), is the result of the implicit infinitely wide distribution of anelastic relaxation times. This example is the least-squares fit of eqns [3] and [9]–[11] to forced-oscillation data for mild steel at tested at 1300°C and 200 MPa. (e) Another example of a broad absorption band, here for melt-free Fo_{90} olivine. The data indicated by the plotting symbols are compared with the generalized Burgers model (eqns [4], [8], [10], and [11]) fitted to such data for a suite of four genuinely melt-free olivine polycrystals. See Faul and Jackson (2005) for details.

where $\Gamma(1+n)$ is the Gamma function (Findley *et al.*, 1976; Gribb and Cooper, 1998a).

From these analytical expressions for $\mathcal{J}_1(\omega)$ and $\mathcal{J}_2(\omega)$, the shear modulus

$$G(\omega) = [\mathcal{J}_1^2(\omega) + \mathcal{J}_2^2(\omega)]^{-1/2} \quad [10]$$

and the associated strain energy dissipation

$$Q^{-1}(\omega) = \mathcal{J}_2(\omega)/\mathcal{J}_1(\omega) \quad [11]$$

are readily evaluated. It follows from eqns [10] and [11] that forced-oscillation measurements of $G(\omega)$ and $Q^{-1}(\omega)$, like the results of microcreep tests, can be represented by a creep-function model in an appropriately internally consistent manner.

In principle, then, knowledge of the creep function $\mathcal{J}(t)$ for arbitrary t and of the dynamic compliance $\mathcal{J}^*(\omega)$ for arbitrary ω provide equivalent insight into the mechanical behavior of the material. Conversion from one description to the other proceeds through integral transforms such as eqn [4] known as the Kronig–Kramers relations (e.g., Nowick and Berry, 1972, p. 37). These alternative descriptions of the mechanical behavior in the time and frequency domains are naturally associated with microcreep and forced oscillation experiments, respectively. Practical considerations related to the acquisition and processing of forced oscillation and microcreep data transform the nature of the relationship between the two methods from strict equivalence to complementarity. Thus, the intensively sampled relatively short-period (< 1–1000 s) stress- and strain-versus-time sinusoids of forced-oscillation experiments can be filtered very effectively with Fourier techniques to yield precise determinations of the relative amplitudes and phase of the stress and strain and hence $\mathcal{J}^*(\omega)$. For periods longer than 1000 s, however, the acquisition of forced-oscillation records representing a substantial number of oscillation periods becomes prohibitively time consuming. It is here that the microcreep method has an important advantage. In addition, the capacity to test explicitly the extent of the recovery of the nonelastic strain following removal of the steady stress is a major advantage of the microcreep method.

Thermodynamic description of anelasticity is based on the notion that stress σ and strain ε are linked not only directly through the unrelaxed modulus $G_U = \mathcal{J}_U^{-1}$, but also indirectly through a third, internal, variable p (Nowick and Berry, 1972; **Figure 3**). If the following conditions are met, the behavior is that of the standard anelastic solid: (1) there exists an equilibrium value $p_0(\sigma)$ of p that is proportional to σ (in the absence of an equilibrium value, the behavior is viscous); (2) $\partial p/\partial t \propto p(t) - p_0$; and (3) the delayed contribution to the strain is proportional to p. There are many different types of internal variable potentially associated with anelastic behavior in geological materials. These include the spatial arrangement of point defects or instantaneous position of a mobile segment of a dislocation line, the position of a mobile twin-domain wall, pressure in an intergranular fluid phase that is spatially variable at the grain or larger scale, and the proportions and chemical compositions of coexisting mineral phases. Many of these possibilities have been considered elsewhere (e.g., Jackson and Anderson, 1970; Karato and Spetzler, 1990). In this review attention will be focused on those mechanisms most likely to exhibit substantial relaxation strength ($\Delta > 0.001$) at teleseismic and lower frequencies (sub-Hz) under the pressure–temperature conditions of the Earth's deep interior.

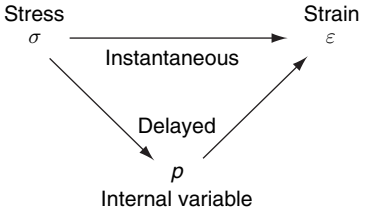

Figure 3 The thermodynamic basis for anelasticity. A third variable p provides an additional indirect and time-dependent link between stress and strain. Redrawn after Nowick and Berry (1972).

2.17.2.2 Intragranular Processes of Viscoelastic Relaxation

The stress-induced migration or redistribution of defects with thermally activated mobility results in viscoelastic behavior even of single crystals when mechanically tested at sufficiently high temperatures. Such defects include vacancies, interstitials, substitutional impurity atoms, and dislocations.

2.17.2.2.1 Stress-induced rearrangement of point defects

Strain–energy dissipation peaks unambiguously associated with the stress-induced migration of point defects have been documented in metals (e.g., Nowick and Berry, 1972). Examples include the stress-induced reorientation of solvent–solute pairs in face-centered cubic (f.c.c.) and other metallic solid solutions (the Zener relaxation), redistribution of C and other small interstitial atoms in body-centered cubic (b.c.c.) metals

such as Fe (the Snoek relaxation) and the stress-induced H diffusion on grain or specimen scale (the Gorsky effect). Such effects might also be expected in mantle minerals – for example, stress-induced repartitioning of Mg and Fe between nonequivalent crystallographic sites. However, relaxation times will generally be very short at mantle temperatures (e.g., <10 ms at 1000°C for Mg/Fe reordering between adjacent M1 and M2 sites in olivine, Aikawa *et al.*, 1985) and relaxation strengths are typically $<10^{-3}$ (Karato and Spetzler, 1990).

2.17.2.2.2 Stress-induced motion of dislocations

Dislocation glide has long been recognized as an important mechanism of viscoelastic relaxation in crystalline solids. Theoretical models of the anelasticity associated with the reversible stress-induced glide of dislocation segments located between adjacent pinning points were first developed in the 1950s to explain low-temperature (<0°C) internal friction peaks in deformed f.c.c. metals (Koehler, 1952; Seeger, 1956; Granato and Lücke, 1956). Although there was general agreement on the relatively large relaxation strength for this process, the characteristic timescale for the stress-induced motion proved more difficult to estimate reliably because of its dependence on structure and chemical composition of the dislocation core and the interactions amongst dislocations and between dislocations and impurities.

2.17.2.2.2.(i) The vibrating-string model of dislocation damping An applied shear stress σ exerts a force σb per unit length on a suitably oriented dislocation of Burgers vector b, causing an initially straight dislocation segment to bow out in its glide plane (**Figure 4(a)**). This tendency is opposed by the line tension or elastic strain energy per unit length

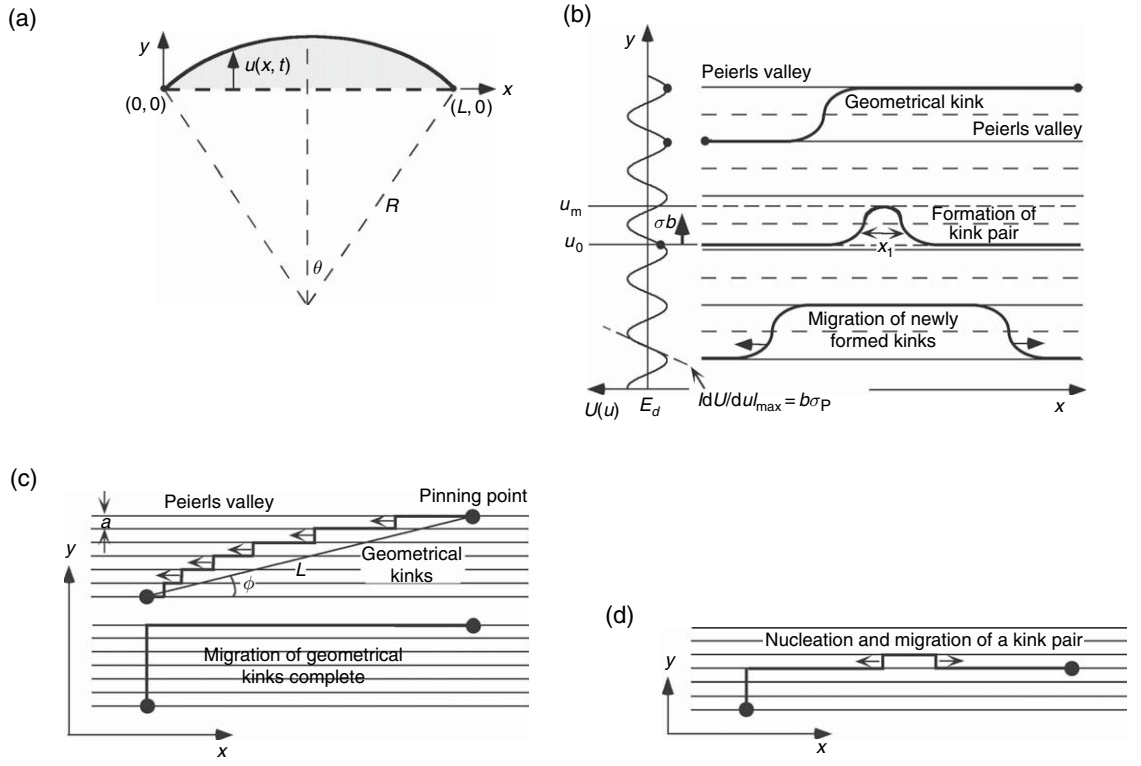

Figure 4 Stress-induced glide of a dislocation segment in response to an externally imposed shear stress σ_{yz} (involving forces parallel to $+y$ ($-y$) acting on the upper (lower) faces of a cube straddling the glide plane in the page. (a) The force exerted on the dislocation by the applied stress and the dislocation line tension are in balance when the dislocation segment has bowed out into an arc with a radius of curvature inversely proportional to the applied stress (eqn [12]). (b) Modulation of the energy of a straight dislocation by the periodic Peierls potential $U(u)$ and its role in the nucleation and migration of kinks (redrawn after Seeger, 1981). (c) The stress-induced migration from right to left of geometrical kinks contributes a well-defined maximum anelastic strain (eqn [30]). (d) At moderately high temperature, the formation and migration of kink pairs will contribute additional anelastic strain.

$E_d \sim (1/2)Gb^2$, where G is the (unrelaxed) shear modulus. (The consequences of the periodic variation of the elastic strain energy of the dislocation about its average value E_d with position in the crystal lattice will be discussed in the following section.) The balance between the force exerted by the applied stress and the line tension determines the relationship between stress and radius of curvature R of the bowed-out segment as

$$R\sigma = Gb/2 \qquad [12]$$

(e.g., Nowick and Berry, 1972). Dislocation segments with length $L < L_c = 2R(\sigma) = Gb/\sigma$ bow out stably under the influence of a static stress σ and will be the primary focus of attention here.

Longer segments ($L > L_c$) participate in dislocation multiplication by the Frank–Read mechanism, thereby increasing the dislocation density and facilitating the transition to power-law dislocation creep. The grain size d imposes an absolute upper limit on the length of dislocation segments. In order to completely exclude the possibility of such dislocation multiplication, and thus guarantee linear behavior, it is accordingly required that

$$\sigma/G < b/d \qquad [13]$$

This condition is assessed below where the applicability of the theory of dislocation relaxation to laboratory experiments and to the Earth's interior is considered.

The classic vibrating-string dislocation-damping model of Koehler (1952) and Granato and Lücke (1956) has been revisited in simplified form by Nowick and Berry (1972) (see also Simpson and Sosin (1972), Minster and Anderson (1981), and Fantozzi *et al.* (1982)). A dislocation line with equilibrium orientation parallel to x is pinned by bound impurity atoms or intersections with other dislocations at $x = 0$ and $x = L$ (**Figure 4(a)**) allowing displacement $u(x, t)$ parallel to y in response to an externally applied oscillating shear stress $\sigma = \sigma_0 \exp(i\omega t)$. The equation of motion expressing the force balance on unit length of dislocation is

$$m_l \partial^2 u/\partial t^2 + B\partial u/\partial t - E_d \partial^2 u/\partial x^2 = \sigma b = \sigma_0 b \exp(i\omega t) \qquad [14]$$

(Granato and Lücke, 1956). In this equation, ρ, $m_l \sim \rho b^2$, B, and $-1/\partial^2 u/\partial x^2$ are respectively the crystal density, the effective mass per unit length of dislocation, the drag coefficient, and the instantaneous radius of curvature of the dislocation segment.

Neglecting high-frequency perturbations to the shape of the oscillating line segment (treated by Granato and Lücke (1956)), Nowick and Berry (1972, pp. 413–417) derived the approximate solution

$$u(x, t) = u_0(Lx - x^2)\exp(i\omega t) \qquad [15]$$

where

$$u_0 = (b\sigma_0/2E_d)/[1 - (\omega/\omega_0)^2 + i\omega\tau] \qquad [16]$$

with

$$\omega_0^2 = 12E_d/m_l L^2 \qquad [17]$$

and

$$\tau = BL^2/12E_d \qquad [18]$$

For a population of N_v dislocation segments per unit volume of common length L and thus a dislocation density (length per unit volume)

$$\Lambda = N_v L \qquad [19]$$

the instantaneous value of the anelastic strain, calculated from the area swept out by the population of similarly favorably oriented bowing dislocations, is then

$$\varepsilon_a(t) = (\Lambda b/L)\int_0^L u(x, t)\,dx = (\Lambda L^2/6)bu_0 \exp(i\omega t) \qquad [20]$$

and the resulting anelastic contribution toward the dynamic compliance (eqn [5]) is

$$\begin{aligned}\delta\mathcal{J}(\omega) &= \varepsilon_a(t)/\sigma(t) \\ &= (\Lambda b^2 L^2/12E_d)/[1 - (\omega/\omega_0)^2 + i\omega\tau]\end{aligned} \qquad [21]$$

For frequencies well below the dislocation resonance frequency ω_0 (estimated from eqn [17] as 20 MHz–2 GHz for $L = 1$–100 μm in olivine), the behavior is approximately that of the standard anelastic solid (eqns [7] without the '$1/\eta\omega$' term). For $\Delta << 1$, eqns [10] and [11] thus become

$$\begin{aligned}Q^{-1}(\omega) &= \Delta\omega\tau/(1 + \omega^2\tau^2) \\ \delta G/G &= \Delta/(1 + \omega^2\tau^2)\end{aligned} \qquad [22]$$

with

$$\begin{aligned}\Delta &= \Lambda G b^2 L^2/12E_d = (1/6)\Lambda L^2 \\ \tau &\sim (1/6)BL^2/Gb^2\end{aligned} \qquad [23]$$

2.17.2.2.2.(ii) The role of kinks in dislocation mobility: migration of geometrical kinks However, it is well known that the elastic strain energy of a dislocation is not constant as assumed for the vibrating string model of dislocation motion, but instead varies about the average value E_d with position u within the crystal lattice. The periodic variation

normal to the close-packed direction is known as the Peierls potential $U(u)$ (**Figure 4(b)**). Especially if the Peierls potential is large, as is typical of silicate minerals, it will be energetically favorable for a stationary or moving dislocation line to lie mainly within a series of low-energy Peierls valleys – the individual straight segments being offset a distance a by kinks (**Figure 4(b)**). The kink picture of dislocation mobility dates from the mid-1950s (Seeger, 1956; Brailsford, 1961; Seeger and Wüthrich, 1976) and has been comprehensively reviewed by Seeger (1981).

We first consider abrupt kinks (of zero width), for which the position $u(x)$ of a dislocation segment of length L is given by

$$u(x) = \int_0^L (\rho_k^- - \rho_k^+)\mathrm{d}x \qquad [24]$$

where ρ_k^- and ρ_k^+ are the numbers of kinks of opposite sign per unit length of dislocation line. Brailsford (1961) expressed the kink densities as functions of x and t that satisfy continuity equations allowing for the thermal generation and recombination of kinks and for their stress-induced migration and diffusion (with mobility and diffusivity μ_k and D_k, respectively). In this way, he derived a differential equation for the motion of the dislocation segment analogous to eqn [14] with the inertial term neglected

$$\partial u/\partial t - D_k \partial^2 u/\partial x^2 = \sigma b a^2 \mu_k (\rho_k^- + \rho_k^+) \qquad [25]$$

A series solution, valid to first order in stress $\sigma_0 \exp(i\omega t)$, was obtained by fixing ρ_{k0}^- and ρ_{k0}^+ at their zero-stress levels, ρ_{k0}^-, and ρ_{k0}^+ respectively. The dominant leading term is of the form

$$u(x, t) - u_0 = u_1 \sin(\pi x/L)\exp(i\omega t)/(1 + i\omega\tau_L) \qquad [26]$$

Substitution into eqn [25] and integration with respect to x allows evaluation of the anelastic relaxation time and relaxation strength associated with the motion of pre-existing (geometrical) kinks as

$$\tau = (L/\pi)^2/D_k \sim (L/\pi a_d)^2 \times [v_{k0}\exp(S_m/k)]^{-1}\exp(H_m/kT) \qquad [27]$$

and

$$\Delta = (8/\pi^4)\Lambda L^2(ab^2G/kT) \times a(\rho_{k0}^- + \rho_{k0}^+) \sim (4/5\pi^4)\Lambda L^2(ab^2G/kT) \qquad [28]$$

(Brailsford, 1961; see also Seeger and Wüthrich (1976), Seeger (1981), and Fantozzi *et al.* (1982)). The kink diffusivity D_k in eqn [27] is given approximately by

$$D_k = a_d^2 v_{k0}\exp(-G_m/kT) \qquad [29]$$

where $G_m = H_m - TS_m$ is the free energy of kink migration, v_{k0} is the attempt frequency of dislocation vibration, and $a_d \sim b$ is the period of the kink potential. Equation [28] gives the relaxation strength for a population of dislocations with dislocation density Λ and uniform segment lengths L with an average value of $a(\rho_{k0}^- + \rho_{k0}^+) \sim \tan\phi$ of 1/10 (ϕ is the inclination of the dislocation line from the Peierls valley; Brailsford, 1961).

Importantly, this analysis of dislocation relaxation based on migration of geometrical kinks yields the same key scalings, whereby $\Delta \propto \Lambda L^2$ and $\tau \propto L^2$, as the vibrating string model (Fantozzi *et al.*, 1982; eqns [23]). The mild temperature dependence of Δ arises from the ratio of kink mobility to diffusivity.

From **Figure 4(c)**, it is clear that the maximum area swept out by migration of geometrical kinks on a dislocation segment of length L is given by $L^2 \sin\phi\cos\phi/2$. The maximum anelastic strain resulting from the migration of geometrical kinks

$$\varepsilon_m = b\Lambda L \sin\phi\cos\phi/2 \qquad [30]$$

(e.g., Karato, 1998) will be compared with the strains of laboratory experiments and seismic wave propagation in a later section.

2.17.2.2.2.(iii) The role of kinks in dislocation mobility: formation and migration of kink pairs

The more elaborate analysis of Seeger (1981) includes a quantitative description of the finite width of kinks and the formation and migration of new kink pairs in the stressed crystal. The starting point is the time-independent force balance per unit length of dislocation (c.f. eqn [14]) with the additional restoring force tending to constrain dislocation segments to lie in the Peierls valleys

$$E_d \mathrm{d}^2u/\mathrm{d}x^2 - \mathrm{d}U/\mathrm{d}u + \sigma b = 0 \qquad [31]$$

Under a static stress σ, a straight dislocation in equilibrium will thus occupy a position u_0 such that

$$(\mathrm{d}U/\mathrm{d}u)|_{u=u_0} = b\sigma \qquad [32]$$

and the maximum value of $|\mathrm{d}U/\mathrm{d}u|$ is thus associated with the Peierls stress σ_P (**Figure 4(b)**).

A more general solution involving kinks is sought by rewriting $\mathrm{d}^2u/\mathrm{d}x^2$ in eqn [31] as $-(1/f^3)\mathrm{d}f/\mathrm{d}u$, where $f = \mathrm{d}x/\mathrm{d}u$. Integration then yields

$$1/f^2 = (2/E_d)\int_{u_0}^{u_m}[\mathrm{d}U/\mathrm{d}u - \sigma b]\mathrm{d}u = (2/E_d)[U(u_m) - U(u_0) - \sigma b(u_m - u_0)] \qquad [33]$$

The requirement that $1/f(u_m)=0$ means that u_m must satisfy

$$U(u_m) - U(u_0) - \sigma b(u_m - u_0) = 0 \qquad [34]$$

with the understanding that for $\sigma=0$, $u_0=0$, and $u_m=a$.

The shape of either a positive or negative geometrical kink ($\sigma=0$) or a kink pair ($\sigma \neq 0$) is then obtained by further integration as

$$x - x_0 = \int_{u_0}^{u_m} f(u)\mathrm{d}u = \pm(2/E_d)^{-1/2} \int_{u_0}^{u_m} [U(u) - U(u_0) - \sigma b(u-u_0)]^{-1/2}\mathrm{d}u \qquad [35]$$

This powerful general result (Seeger, 1981, eqn [5]) provides the basis for a detailed description of the role of kinks in anelastic relaxation. Both pre-existing (geometrical) kinks and newly formed kink pairs may contribute. The following is a brief outline of the way in which estimates of relaxation strength Δ and relaxation time τ have been derived through considerations based on eqn [35]. In order to illustrate key aspects of the theory, some results are evaluated for a specific (sinusoidal) functional form for the Peierls potential

$$U(u) = U(0) + (a/2\pi)b\sigma_P[1 - \cos(2\pi u/a)] \qquad [36]$$

along with the approximations $a \sim b$ and $E_d \sim (1/2)Gb^2$.

The energy of formation H_k and width w_k of a single geometrical kink are

$$H_k = \int_{-\infty}^{\infty} \{E_d[\mathrm{d}s/\mathrm{d}x - 1] + [U(u) - U(0)]\}\mathrm{d}x = (2E_d)^{1/2} \int_0^u [U(u) - U(0)]^{1/2}\mathrm{d}u \qquad [37]$$

with $\mathrm{d}s = (\mathrm{d}x^2 + \mathrm{d}u^2)^{1/2}$ and

$$w_k = a|\mathrm{d}x/\mathrm{d}u|_{u=a/2} = 2a^2E_d/\pi H_k \qquad [38]$$

For the sinusoidal Peierls potential (eqn [36]), these expressions can be evaluated as

$$H_k = (2a/\pi)(2ab\sigma_P E_d/\pi)^{1/2} \sim (2/\pi^{3/2})Gb^3(\sigma_P/G)^{1/2} \qquad [39]$$

and

$$w_k = (\pi^{1/2}/2)b(\sigma_P/G)^{-1/2} \qquad [40]$$

The functional forms of eqns [39] and [40] illustrate the close relationship between the Peierls stress and the geometry and energetics of kink formation. The higher the Peierls stress, the narrower are the kinks and the greater is their formation energy.

Allowance for the work done against the external stress in forming a kink pair yields

$$H_{kp} = 2(2E_d)^{1/2} \int_{u_0}^{u_m} [U(u) - U(u_0) - \sigma b(u-u_0)]^{1/2}\mathrm{d}u < 2H_k \qquad [41]$$

An estimate of the kink-pair formation energy that is more accurate for low stress conditions ($\sigma/\sigma_P << 1$) corresponds to the unstable equilibrium spacing x_1 of kinks of opposite sign at which their interaction energy H_{int} is maximized:

$$H_{kp} = 2H_k - H_{int}(x_1) \qquad [42]$$

Under these conditions, there is a balance between the forces associated with the applied stress and with the long-range elastic interaction seeking respectively to increase and decrease the kink separation (**Figure 4(b)**).

Analysis of the statistical mechanics of the dislocated crystal (with and without kinks) leads to estimates of the entropy of kink formation, the kink-pair formation rate, and hence the equilibrium density of kinks of given sign per unit length of dislocation line, given by

$$\rho_k^{eq} = (1/w_k)(2\pi H_k/kT)^{1/2}\exp(-H_k/kT) \qquad [43]$$

(for the sinusoidal potential). The velocity of a dislocation moving perpendicular to its Peierls valley by the formation and separation of kink pairs is then calculated. Finally, expressions are obtained for the relaxation strength

$$\Delta = \Lambda L^2 b^2 G_u/12E_d \sim (1/6)\Lambda L^2 \qquad [44]$$

and the relaxation time

$$\tau = [kT/(\rho_k^{eq})^2 D_k](L/2a^2E_d)(1 + \rho_k^{eq}L) \qquad [45]$$

(eqns [45] and [50] of Seeger (1981)). The latter applies to conditions of stress sufficiently low for the temperature-dependent equilibrium kink density to be maintained and for all but very low temperatures (<10 K). It follows from eqns [29], [43], and [45] that different effective activation energies of approximately $2H_k + H_m$ and $H_k + H_m$, respectively, are expected for the low- and high-temperature regimes defined by $\rho_k^{eq}L << 1$ and $\rho_k^{eq}L >> 1$, respectively. The lower activation energy $H_k + H_m$ for the high-temperature regime reflects the greater probability of kink annihilation at high kink densities.

The relaxation strength (eqn [44]) is identical to that for the vibrating string model (eqn [23]) as expected from geometrical considerations. At the high kink densities of the high-temperature regime

($\rho_k{}^{eq}L >> 1$), the relaxation time given by eqn [45] is equivalent to eqn [23] for the vibrating string model with the drag coefficient $B = 6kT/\rho_k{}^{eq}D_k a^2$, reasonably, inversely proportional to the product of the kink density and kink mobility (D_k/kT).

2.17.2.2.2.(iv) Relaxation strength for dislocation damping The foregoing analysis (eqns [23] and [44]) yields a substantial relaxation strength $\Delta \sim 0.1$–1 for the stress-induced migration of favourably oriented intragranular dislocation segments with the dislocation density $\Lambda \sim L^{-2}$ of a three-dimensional (3-D) (Frank) network. A relaxation strength of order unity for olivine at upper-mantle temperatures is similarly expected from eqn [28] for relaxation due to the motion of geometrical kinks if the dislocation density approaches that of the Frank network. Somewhat lower values of $\Delta \sim 0.01 - 0.1$ are inferred once allowance is made for more typical geometries. However, for dislocations closely spaced (separation h) in the walls of subgrains of dimension L, the predicted relaxation strength is enhanced relative to that for a Frank network by the factor L/h which can be substantially greater than 10 (Friedel *et al.*, 1955; Nowick and Berry, 1972).

2.17.2.2.2.(v) Absorption band behavior: distribution of relaxation times The foregoing theory is readily generalized to accommodate a wide distribution of dislocation segment lengths (e.g., Schoeck, 1963). If $p_L(L)\mathrm{d}L$ is the number of dislocation segments per unit volume of length between L and $L + \mathrm{d}L$, then the total dislocation length per unit volume is

$$\Lambda = \int_0^\infty p_L(L) L \, \mathrm{d}L \qquad [46]$$

The internal friction and frequency-dependent modulus are, respectively,

$$Q^{-1}(\omega) = \Delta \int_0^\infty p_L(L) L^3 \omega\tau(L) \mathrm{d}L / [1 + \omega^2\tau^2(L)] \qquad [47]$$

and

$$G(\omega)/G_u = 1 - \Delta \int_0^\infty p_L(L) L^3 \mathrm{d}L / [1 + \omega^2\tau^2(L)] \qquad [48]$$

where Δ is now the anelastic relaxation strength for the entire distribution of dislocation segment lengths.

For geological materials tested in the laboratory, the dissipation commonly displays a monotonic variation of Q^{-1} with frequency and temperature represented by

$$Q^{-1} \sim [\omega \exp(E/RT)]^{-\alpha} \qquad [49]$$

with $\alpha \sim 0.3 \pm 0.1$ (Berckhemer *et al.*, 1982; Jackson *et al.*, 2002). Geophysical observations of the attenuation of seismic body and surface waves and free oscillations, and of strain–energy dissipation at the longer periods of earth tides and the Chandler wobble, are broadly consistent with this view of the frequency dependence of Q^{-1} (e.g., Minster and Anderson, 1981; Shito *et al.*, 2004). If eqn [47] with $\tau(L) \sim L^2$ (e.g., eqns [23], [27], and [45]) is to yield $Q^{-1} \sim \omega^{-\alpha}$, it is required that the distribution of dislocation segment lengths adopt the form

$$p_L(L) \sim L^{2\alpha - 4} \qquad [50]$$

strongly skewed toward short dislocation lengths (Minster and Anderson, 1981; Karato, 1998). Alternatively, or additionally, a distribution of activation energies for dislocation migration might contribute to the breadth of an anelastic absorption band (Minster and Anderson, 1981).

2.17.2.2.2.(vi) Dislocation relaxation: transition from anelastic to viscous behavior The foregoing analysis is based on the assumption that dislocation segments are firmly pinned by bound impurities and/or interactions with other dislocations. Under these circumstances, the restoring force provided by line tension or recovery of kink-pair formation energy ensures that the nonelastic strain is recoverable upon removal of the applied stress, meaning that the behavior is anelastic. However, at sufficiently high temperatures and/or stress amplitudes, dislocation segments may break free from their pinning points, thereby allowing larger, irrecoverable (viscous) strains. By balancing the work done in moving the dislocation away from the pinning point with the binding energy E_{up} of the dislocation to the pinning point, the critical stress σ_{up} for unpinning (at 0 K) can be estimated as

$$\sigma_{up} = E_{up}/abL \qquad [51]$$

For finite temperature T, thermal activation will allow unpinning at somewhat lower stresses with a probability proportional to $\exp[-(E_{up} - \sigma abL)/kT]$ (Nowick and Berry, 1972, pp. 364–365).

2.17.2.2.2.(vii) Role of water in nominally anhydrous minerals The presence of intragranular water (or more accurately hydrogen-related defects) is known to affect both large-strain rheology

and electrical conductivity of nominally anhydrous silicate minerals like olivine and wadsleyite. Arguing mainly by analogy with such observations, Karato and Jung (1998) suggested that the concentration C_{OH} of hydroxyl within mineral grains and/or grain boundaries might similarly enhance seismic wave attenuation and dispersion through its influence on the concentrations and mobilities of key defects. For parametrization they suggested a variant of eqn [49]:

$$Q^{-1} \sim [(A + BC_{OH})/\omega \exp(gT_m/T)]^{\alpha} \qquad [52]$$

in which T_m is the relevant melting temperature and g is a dimensionless constant.

2.17.2.3 Intergranular Relaxation Processes

2.17.2.3.1 Effects of elastic and thermoelastic heterogeneity in polycrystals and composites

The role of the heterogeneous microscopic stress field that arises in stressed polycrystals as the inevitable consequence of the elastic anisotropy of the component crystallites has been somewhat neglected in discussions of the nature of the high-temperature internal friction background. During testing under conditions of high temperature and low frequency, these intergranular fluctuations in stress may be subject to relaxation by the reversible migration of grain boundaries (Leak, 1961). Such grain-boundary migration is driven by the minimization of the elastic strain energy of the stressed polycrystal (Kamb, 1959). The anelastic relaxation involves enlargement of those grains oriented for high compliance under the prevailing stress relative to neighboring grains oriented for lower compliance (Nowick and Berry, 1972, p. 453; **Figure 5**).

A useful indication of the magnitude of the modulus relaxation (Kumazawa, 1969) derives from consideration of the physical basis for the Voigt and Reuss bounds on the effective elastic moduli of a polycrystal. In such discussions, the Reuss (lower) bound on the effective moduli assumes special significance because it corresponds to a state of uniform stress throughout the polycrystal. It is just this condition that is approached through relaxation of the initially inhomogeneous internal stress field. Kumazawa therefore concluded that the difference between the Voigt–Reuss–Hill (or the average G_{HS} of the more closely spaced Hashin–Shtrikman bounds) and Reuss averages (G_{RS}) of the single-crystal elastic constants is a measure of the inherent nonelastic behavior of the polycrystal. Thus, the fractional relaxation of the shear modulus is given by

$$\delta G/G = (G_{HS} - G_{RS})/G_{HS} \qquad [53]$$

Shear moduli intermediate between G_{HS} and G_{RS} can accordingly be achieved through the relaxation toward uniformity of the inhomogeneous internal stress field arising from the elastic anisotropy of the individual crystallites.

Elastic heterogeneity in polycrystals and multiphase composites leads also to bulk dissipation Q_K^{-1} arising from the coupling between macroscopic volumetric strain and internal shear strains (Budiansky and O'Connell, 1980). Their estimates of Q_K^{-1}/Q_G^{-1} for representative upper-mantle materials will be considered in Section 2.17.4. The magnitude of Q_K^{-1} and the extent of the associated relaxation of the bulk modulus depend on the spacing between the HS-average and Reuss bounds on the effective bulk modulus (c.f. eqn [53]). These are typically much more closely spaced than for the shear modulus resulting in more modest anelastic relaxation of the bulk modulus (Section 2.17.4).

Anisotropy and inter-phase variability (collectively, heterogeneity) of elastic constants and thermal expansivity within polycrystals and composite materials result in spatial heterogeneity of the temperature changes caused by adiabatic compression, that may be relaxed toward isothermal conditions by intergranular or inter-phase heat flow (Zener, 1952; Budiansky *et al.*, 1983). A formal phenomenological theory (Zener, 1952, pp. 84–89) for such thermoelastic behavior, valid at frequencies sufficiently high for the diffusion of heat to be confined to the immediate neighborhood of the grain or inter-phase boundaries, yields

$$Q^{-1} \sim A(D/\omega)^{1/2}/d \qquad [54]$$

(cf. eqn [49]), where D is the thermal diffusivity and d is the grain size. The dissipation scales with the measure A of the heterogeneity of the relevant physical property. The relevance of thermoelastic

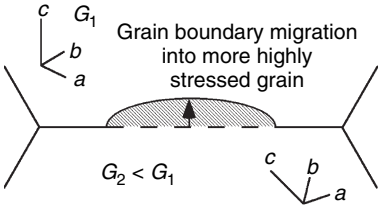

Figure 5 Reversible stress-induced grain-boundary migration as an anelastic relaxation mechanism. The driving force for the (normal) migration of the boundary is the reduction of elastic strain energy. Redrawn after Jackson *et al.* (2000).

damping to bulk dissipation Q_K^{-1} in the Earth's mantle will be considered briefly in Section 2.17.4.

2.17.2.3.2 Grain-boundary sliding

2.17.2.3.2.(i) Overview Grain-boundary sliding has been widely invoked as a plausible mechanism for the ubiquitous transition from elastic through anelastic to viscous behavior in fine-grained polycrystalline materials. Central to the theory of grain-boundary sliding is the notion of a grain boundary region, of finite width δ, distinguished from the crystalline lattices of the neighboring grains by a higher degree of positional disorder, and consequently, higher diffusivities D_b for the various atomic and molecular species and lower viscosity η_b. At sufficiently low-temperature and/or high-frequency, grain-boundary sliding will be inhibited, and an unrelaxed shear modulus G_U representative of the strictly elastic behavior of the polycrystal is expected (**Figure 6**, uppermost panel). With increase of temperature and/or timescale of the mechanical test beyond an appropriate threshold, it is envisaged that relaxation (to zero) of the distribution of grain-boundary shear stress allows a finite amount of sliding along suitably oriented boundaries accommodated by elastic distortion of the neighboring grains (Ashby, 1972). The modified distribution of normal stress associated with the accommodating elastic distortion provides the restoring force required for macroscopically anelastic (i.e., recoverable) behavior (**Figure 6**, middle panel). At still longer timescales and higher temperatures, it is envisaged that viscous deformation occurs with grain-boundary sliding accommodated by diffusional transport of matter away from boundary regions of high chemical potential (normal stress) to other parts of the grain boundary at lower chemical potential (Raj and Ashby, 1971). The transition from the anelastic behavior associated with elastically accommodated grain-boundary sliding to steady-state viscous behavior requires an adjustment of the distribution of normal stress that is facilitated by grain-boundary diffusion (**Figure 6**, lowermost panel).

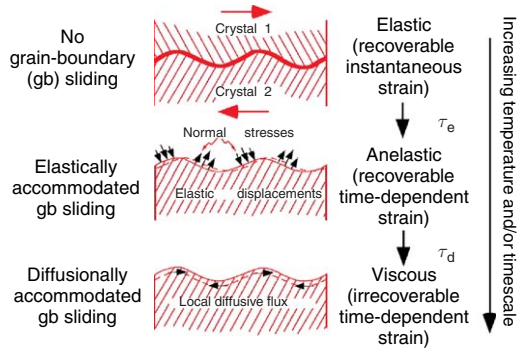

Figure 6 Grain-boundary sliding as a viscoelastic relaxation mechanism. The low effective viscosity of the grain-boundary region facilitates local shear stress relaxation and sliding providing for a seamless transition with increasing temperature and/or timescale from elastic through anelastic to viscous behavior as described in the text. Adapted from Ashby MF (1972) Boundary defects and atomistic aspects of boundary sliding and diffusional creep. *Surface Science* 31: 498–542.

2.17.2.3.2.(ii) Elastically accommodated grain-boundary sliding The elastic regime prevailing following completion of elastically accommodated sliding was analyzed in the classic work of Raj and Ashby (1971). The component of the normal stress parallel to the mean direction x of the grain boundary and integrated over the wavelength λ of the periodic boundary balances the externally applied shear stress σ. The elastic strains caused by the newly created distribution of normal stress are those required to restore grain shape compatibility across the slipped boundary. With the boundary topography $u(x)$ for a 2-D array of hexagonal grains (of unrelaxed shear modulus G_U and Poisson's ratio ν) represented by a Fourier series

$$u(x) = \sum_{j=1}^{\infty} h_j \cos(2\pi jx/\lambda) \qquad [55]$$

the following expressions were obtained for the normal stress σ_n and the equilibrium distance U of reversible sliding:

$$\sigma_n(x) = -\sigma\lambda \sum_{j=1}^{\infty} j^2 h_j \sin(2\pi jx/\lambda) \Big/ \left[\pi \sum_{j=1}^{\infty} j^3 h_j^2\right] \qquad [56]$$

$$U = (1-\nu)\lambda^3\sigma \Big/ \left[2\pi^3 G_U \sum_{j=1}^{\infty} j^3 h_j^2\right] \qquad [57]$$

Numerical results, apparently based on truncation of the infinite series after $N = 100$ terms, yielded a finite sliding distance and a corresponding large anelastic relaxation strength

$$\Delta = 0.57(1-\nu) \qquad [58]$$

independent of grain size. For example, for $\nu = 0.26$, appropriate for olivine at 1000–1300°C (Anderson and Isaak, 1995), $\Delta \sim 0.42$. The relaxed shear modulus G_R and the height Q_D^{-1} of the Debye dissipation peak (as appropriate for the standard anelastic solid) are given by the following expressions:

$$G_R/G_U = 1/(1+\Delta), \quad Q_D^{-1} = (\Delta/2)/(1+\Delta)^{1/2} \qquad [59]$$

However, because $h_j \sim j^{-2}$ (Raj, 1975), the infinite sum $\Sigma\, j^3 h_j^2$ in the denominators of eqns [56] and [57] fails to converge – suggesting that sufficiently sharp grain-edge intersections might inhibit elastically accommodated sliding (Faul *et al.*, 2004; Jackson *et al.*, 2006). The higher values of $\Delta \sim 0.8$ obtained in the modeling of sliding between spherical grains (Zener, 1941; Kê, 1947) and the lower values (0.23 for $v = 0.26$) reported from a finite-element study with a fine mesh (Ghahremani, 1980) are consistent with this suggestion.

The relaxation time for elastically accommodated grain-boundary sliding is given by

$$\tau_e = \gamma \eta_b d / G_U \delta \qquad [60]$$

where γ, of order 1, is either a constant or a function of Poisson's ratio v for the unrelaxed material (Kê, 1947; Nowick and Berry, 1972; Mosher and Raj, 1974; O'Connell and Budiansky, 1977; Ghahremani, 1980).

2.17.2.3.2.(iii) Diffusionally accommodated grain-boundary sliding The possibilities of elastic and steady-state diffusional accommodation of grain-boundary sliding were examined separately by Raj and Ashby (1971). Grain-boundary sliding with 'sequential' occurrence of elastic and diffusional accommodation was explored by Raj (1975) in his analysis of transient diffusional creep. The transient required to adjust the normal stress distribution from that prevailing on completion of elastically accommodated sliding (eqn [56]) to that required for steady-state diffusional creep is of approximate duration

$$\tau_d = (1 - v) k T d^3 / [40 \pi^3 G_U \delta D_b \Omega] \qquad [61]$$

Ω is the molecular volume of the diffusing species and D_b is the grain-boundary diffusivity. The transient creep rate calculated by Raj is enhanced relative to the corresponding steady-state diffusional creep rate by a numerical factor that varies approximately as $(t/\tau_d)^{-1/2}$, which integrates to a creep function of the Andrade form (eqn [3]) – as recognized and emphasized by Gribb and Cooper (1998a; see also Cooper (2003)). This creep function implicitly involves a monotonic and infinitely wide distribution of anelastic relaxation times (Jackson, 2000) and therefore does not result in a dissipation peak. The diffusional creep transient should instead be responsible for a wide absorption band, within which

$$Q^{-1} \sim T_o^{1/2} d^{-s} \qquad [62]$$

with period $T_o = 2\pi/\omega$ and $1 < s < 3/2$ (Gribb and Cooper, 1998a; Faul *et al.*, 2004).

Through use of the well-known connection between grain-boundary diffusivity and viscosity, it can be shown that $\tau_e/\tau_d << 1$. Thus, it is predicted that the dissipation peak associated with the transition between elastic and anelastic behavior and the onset of appreciable distributed dissipation associated with the progressive transition between anelastic and viscous behavior should be widely separated in oscillation period – temperature space (Jackson *et al.*, 2002).

However, a consistent pattern of high-temperature viscoelastic behavior at variance with the classic Raj–Ashby theory is emerging from intensive laboratory studies on fine-grained geological and ceramic materials (Section 2.17.3). These observations have provided the motivation for a new approach to the micromechanical modeling of grain-boundary sliding free from the principal limitations of Raj–Ashby theory, namely that elastic and diffusional accommodation occur separately and sequentially, and that grain edges are only moderately sharp (Jackson *et al.*, 2006). The boundary-value problem incorporating both sliding and diffusion has been solved with a perturbation approach, valid only for a gently sloping periodic boundary, providing for the first time, the complete relaxation spectrum (Morris and Jackson, 2006). As expected, the boundary viscosity determines the behavior at short periods T_o – with Q^{-1} increasing with increasing T_o toward the elastically accommodated sliding peak of classical theory (Raj and Ashby, 1971). Further increase of T_o leads to a regime beyond the peak where grain-boundary diffusion dominates – its influence extending progressively with increasing period from relaxation of stress concentrations at grain corners, where Q^{-1} varies only mildly with period, ultimately to grain-scale diffusion associated with steady-state creep ($Q^{-1} \sim T_o$). Significantly, the peak height varies inversely with the boundary slope, but a final answer for finite boundary slope with arbitrarily sharp grain-edge intersections awaits the results of numerical analysis in progress.

Finally, in the context of diffusional creep it should be stressed that free surfaces, grain boundaries, polygonized (subgrain) boundaries, and even individual dislocations act as easy sources and sinks of vacancies. Stress-induced migration of vacancies results in diffusional creep with a strain rate

$$d\varepsilon/dt = \gamma D \sigma b^3 / d^2 k T \qquad [63]$$

where d is the characteristic separation of vacancy sources and sinks which can be substantially smaller than the grain size and the dimensionless constant γ is of order unity (Friedel, 1964, pp. 311–314). It was suggested by Friedel that such diffusional creep might be an important contributor to the high-temperature internal friction background. However, as a viscous process it would result in a stronger frequency dependence $Q^{-1} \sim \omega^{-1}$ than is observed experimentally (see below).

2.17.2.4 Relaxation Mechanisms Associated with Phase Transformations

2.17.2.4.1 Stress-induced variation of the proportions of coexisting phases

Relaxation associated with stress-induced change of the proportions of coexisting crystalline or solid and liquid phases has been analyzed in detail by Darinskiy and Levin (1968) and Vaišnys (1968; see also Jackson and Anderson (1970)). The following simplified treatment is intended to explain the nature of such relaxation. Consider a region of pressure (P)–temperature (T)–bulk composition (X) space within which two phases such as a pair of low- and high-pressure polymorphs with density contrast $(\delta\rho/\rho)_0$ coexist in thermodynamic equilibrium. A superimposed small fluctuation p_s in pressure (under isothermal conditions), arising for example, from a seismic compressional wave will induce changes in the equilibrium proportions and compositions of the coexisting phases. If the width of the two-phase region is δP (for given T and X), the magnitude of the implied fractional density perturbation is approximately

$$\varepsilon_a = (\delta\rho/\rho)_a = (p_s/\delta P)(\delta\rho/\rho)_0 \qquad [64]$$

The volumetric strain specified by eqn [64] is proportional to the pressure perturbation and the attainment of the perturbed equilibrium will require finite time for diffusional rearrangement of the various chemical species. Moreover, the process is reversible on removal of the pressure perturbation. The conditions for anelastic behavior (identified above) are thus clearly satisfied. The corresponding elastic strain is given by

$$\varepsilon_e = (\delta\rho/\rho)_e = p_s/\underline{K} \qquad [65]$$

where $\underline{K}(X, T)$ is the appropriate average of the unrelaxed bulk moduli for the coexisting phases. The relaxation strength, given by the ratio $\varepsilon_a/\varepsilon_e$ of the anelastic and elastic strains as in eqn [4], is thus

$$\Delta_v = (\underline{K}/\delta P)(\delta\rho/\rho)_0 \qquad [66]$$

Because $\underline{K}/\delta P$ can be very large, Δ_v can be substantial (>1) even for a modest density contrast of order 0.01 (Vaišnys, 1968). The thermodynamic coexistence of the two phases, especially in subequal proportions near the middle of the two-phase loop, presumably means that nucleation is no barrier to further incremental transformation in either direction. An increase in the volume fraction of whichever phase is favored by the instantaneous value of the fluctuating hydrostatic pressure at the expense of the other phase would presumably be accomplished most readily by the migration normal to itself of the phase boundary across which grains of the two phases are in contact. The adjustment $\sim p_s/\delta P$ to the proportions of the coexisting phases could then be accomplished by multicomponent diffusion with a diffusivity D given approximately by that of the most slowly diffusing major-element species (usually Si in silicate minerals). For equal proportions of the two phases, the necessary change in volume requires the formation of an outer rind of thickness

$$\delta \sim (d/3)(p_s/\delta P) \qquad [67]$$

on an approximately spherical grain of diameter d. If diffusion were the rate-controlling step, the relaxation time would thus be of order

$$\tau \sim \delta^2/D(T) = (d^2/9D_0)(p_s/\delta P)^2 \exp(H/RT) \qquad [68]$$

In this simple analysis several major sources of complication have been ignored, particularly in estimation of the relaxation time. No attempt has been made to model the time-dependent stress at the phase boundary or the transformation kinetics, potentially strongly influenced by the rheology of the surrounding medium (Darinskiy and Levin, 1968; Morris, 2002). Nevertheless, the broad feasibility of such relaxation of the bulk modulus for seismic wave propagation in the transition zone will be explored below.

These ideas are also readily applied to stress-induced variations in the proportion of melt in partially molten material. In this case the pressure perturbation p_s slightly modifies the solidus and liquidus temperatures by an amount

$$\delta T_s \sim (\mathrm{d}T_m/\mathrm{d}P)p_s \qquad [69]$$

If δT_0 is the width of the melting interval, then the change to the melt fraction caused by the pressure fluctuation p_s is

$$\delta\phi \sim \delta T_s/\delta T_0 \quad [70]$$

which plays an analogous role to $p_s/\delta P$ in the foregoing analysis (Vaišnys, 1968; Jackson and Anderson, 1970; Mavko, 1980).

2.17.2.4.2 Stress-induced migration of transformational twin boundaries

Another possible mechanism of seismic wave attenuation and dispersion, with particular potential application to the Earth's silicate perovskite-dominated lower mantle (and perhaps parts of the lithosphere), involves the stress-induced migration of boundaries between ferroelastic twins. The ABO_3 perovskite structure relevant to the lower mantle, comprising a 3-D corner-connected framework of cation-centered BO_6 octahedra with larger A cations occupying the cage sites, displays an extraordinary versatility based on the systematic tilting and/or rotation of adjacent octahedra. In this way the structure is not only able to accommodate cations that vary widely in size and charge, but also able to respond flexibly to changing conditions of pressure and temperature. Thus, many perovskites cooled from high temperature undergo a series of displacive phase transformations to structures of progressively lower symmetry, each transition accompanied by the appearance of a spontaneous shear strain. The reduction of symmetry typically results in the formation of a microstructure comprised of transformational twins with different orientations (relative to the lattice of the parent crystal) meeting in domain walls.

The nature of anelastic relaxation associated with the stress-induced motion of such domain walls has been explained by Harrison and Redfern (2002; see also Schaller *et al.*, 2001) as follows. Under an applied stress, the free energy degeneracy between adjacent twin domains is removed resulting in a force acting on the domain wall. Thus, domain walls will tend to migrate so as to enlarge the domains of relatively low free energy at the expense of those of higher energy. The result is an additional nonelastic contribution to the macroscopic strain that is proportional to the product of the spontaneous strain, the density of domain walls, and the distance through which they move. Interactions between domain walls, between domain walls and associated defects, and between domain walls and the surface of a laboratory specimen result in a finite mobility or equivalently a characteristic timescale for their motion that is thermally activated. Moreover, the process of domain wall migration is reversible on removal of the applied stress – meeting the final criterion for anelastic behavior discussed in Section 2.17.2.1.

2.17.2.5 Anelastic Relaxation Associated with Stress-Induced Fluid Flow

The presence within a rock of an intergranular fluid phase creates additional opportunities for anelastic relaxation. Well-developed theoretical models predict the dependence of elastic bulk and shear moduli and attenuation upon the volume fraction and viscosity η_f of the fluid, and upon the nature of the grain-scale fluid distribution and the angular frequency ω of the applied stress field (Walsh, 1968, 1969; O'Connell and Budiansky, 1977; Mavko, 1980; Schmeling, 1985; Hammond and Humphreys 2000a, 2000b; see review by Jackson (1991)).

The model microstructure typically comprises a population of fluid-filled inclusions of specified shape (e.g., ellipsoids, grain-boundary films, or grain-edge tubes) and connectivity embedded within a crystalline matrix, subject to an externally imposed stress field. As a consequence of the distortion of the matrix, each fluid inclusion is exposed to a particular state of stress. Depending upon the frequency of the applied stress, any one of four distinct fluid stress regimes may be encountered: glued, saturated-isolated, saturated-isobaric, and drained, listed here in order of decreasing frequency (O'Connell and Budiansky, 1977; **Figure 7**). The response to an externally imposed shear stress will be considered first. At sufficiently high frequencies, within the glued regime, the fluid is able to support a nonhydrostatic stress with an effective shear modulus $|G| = \omega\eta_f$ not substantially less than the matrix rigidity so that relative tangential displacement of neighboring grains is inhibited and the influence of the fluid is minimal. The saturated–isolated regime, where the fluid no longer supports shear stress but fluid pressure varies between (even adjacent) inclusions of different orientation, is encountered at somewhat lower frequencies. For still lower frequencies, fluid pressures are equilibrated by fluid flow between adjacent inclusions ('melt squirt', Mavko and Nur, 1975) in the saturated–isobaric regime. Finally, at very low frequencies, drained conditions will apply for which no stress-induced perturbation

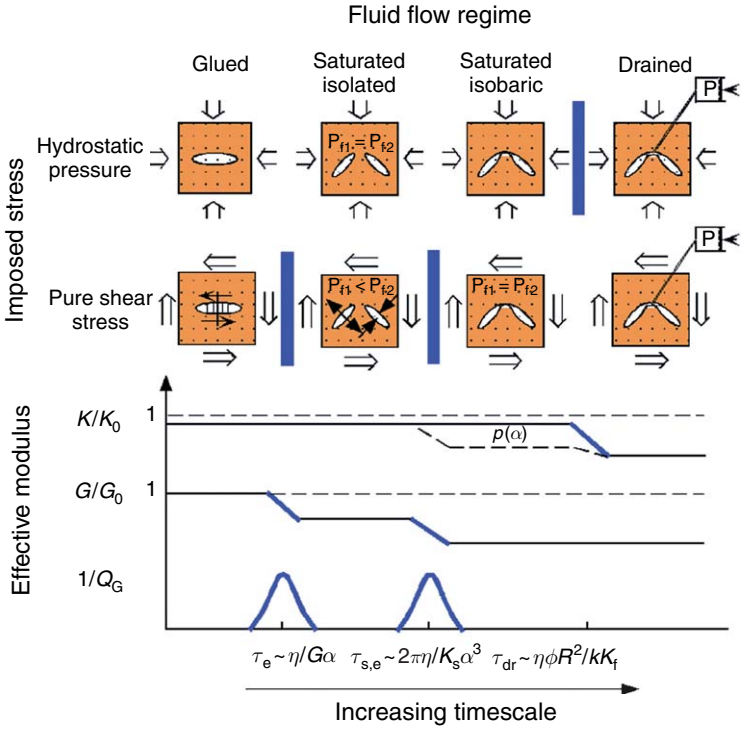

Figure 7 Fluid-flow regimes and effective elastic moduli for a medium containing ellipsoidal fluid inclusions of given aspect ratio α, as envisaged by O'Connell and Budiansky (1977). The upper row of panels shows the response of the medium to hydrostatic compression, whereas the lower row shows the response to shear. The vertical black bars highlight the transitions between fluid-flow regimes that are expected to cause marked modulus relaxation. A distribution $p(\alpha)$ of fluid-inclusion aspect ratios leads to partial relaxation of the bulk modulus in the saturated isobaric regime as indicated by the dashed line within the saturated isobaric regime. P_{f1} and P_{f2} are the pore pressures in representative inclusions of different orientation relative to the applied stress. Adapted from Lu C and Jackson I (2006) Low-frequency seismic properties of thermally cracked and argon saturated granite. *Geophysics* 71: F147–F159.

of pore fluid pressure (relative to that in an external reservoir) can be sustained.

The transition between the glued, saturated–isolated, and saturated–isobaric regimes are possible causes of dispersion and attenuation under the conditions of laboratory petrophysical experimentation and for seismic waves within the Earth's crust and its deeper interior. The transition from the glued regime to the saturated–isolated regime, in which the fluid no longer supports shear stress but undergoes no grain-scale flow, is formally identical to the process of elastically accommodated grain-boundary sliding reviewed above. The grain-boundary fluid inclusion is simply identified with the boundary region of aspect ratio $\alpha_b = \delta/d$ and low viscosity η_b, and the relaxation time is given by eqn [59] rewritten in terms of α_b as

$$\tau_e = \gamma\eta_b/G_u\alpha_b \qquad [71]$$

The relaxation time for fluid squirt between the triple-junction tubules characteristic of a nonwetting melt was estimated by Mavko (1980) as

$$\tau_{s,t} = 160\,\eta_m/K_m\alpha_t^2 \qquad [72]$$

where $\alpha_t = 2R/d$ is the aspect ratio of the tubules (diameter/length), K_m is the bulk modulus of the melt, and η_m the viscosity of the melt. The relaxation time for melt squirt between ellipsoidal inclusions was given by O'Connell and Budiansky (1977) as

$$\tau_{s,e} = 2\pi\eta_m/K_s\alpha_e^3 \qquad [73]$$

where K_s is the bulk modulus of the solid and α_e the aspect ratio (width/length) of the ellipsoidal melt inclusions.

The characteristic timescale for each of these three processes of anelastic relaxation thus depends on the viscosity of the fluid phase (or grain-boundary material) as well as the aspect ratio of the fluid inclusion or grain-boundary region of relatively low viscosity. The variations of relaxation time for representative ranges of aspect ratio and viscosity for each of the three processes are contoured in **Figure 8**. Each line is the locus of all combinations of aspect

ratio and viscosity that yield a particular relaxation time. All combinations (α, η) that plot above (below) a contour corresponding to a given relaxation time τ, are associated with unrelaxed (relaxed) behavior for oscillation period $T_o = \tau$. For a given mechanism to produce a relaxation peak centered within the teleseismic band (1–1000 s), it is therefore required that the relaxation time calculated as a function of aspect ratio and viscosity fall between the 1 and 1000 s contours indicated in **Figure 8**. An interpretation of dissipation data from laboratory experiments on melt-bearing fine-grained olivine polycrystals, based on **Figure 8**, is presented in Section 2.17.3.3.

The effective elastic moduli, and hence relaxation strengths associated with the transitions between these fluid-flow regimes, depend upon both the volume fraction ϕ, and aspect ratio, α (minimum/maximum dimension) of the fluid inclusions. However, for relatively low fluid fractions and low aspect ratios (i.e., fluid-filled cracks rather than pores), the behavior is controlled primarily by a single variable known as crack density, ε (O'Connell and Budiansky, 1974). For a population of spheroidal inclusions of common low aspect ratio, ε is given by

$$\varepsilon = 3\phi/4\pi\alpha \qquad [74]$$

which definition can be generalized to accommodate a distribution of crack aspect ratios.

For the transition between the glued and saturated isolated regimes, the relaxation of the shear modulus is given, for low crack density ε, by

$$\delta G \sim 32(1-v)G\varepsilon/[15(2-v)] = (32/35)G\varepsilon \quad (\text{for } v = 1/4) \qquad [75]$$

For the transition from the saturated isolated regime to the saturated isobaric regime, the further relaxation of the shear modulus is

$$\delta G \sim 32(1-v)G\varepsilon/45 = (8/15)G\varepsilon \quad (\text{for } v = 1/4) \qquad [76]$$

meaning that fluid squirt is only about half as effective as elastically accommodated grain-boundary sliding as a relaxation mechanism (O'Connell and Budiansky, 1977). A nonwetting fluid, confined to grain-edge tubules, is much less effective in reducing the shear modulus in both saturated isolated and saturated isobaric regimes (Mavko, 1980).

As regards the bulk modulus, the presence of fluid inclusions with a bulk modulus K_f substantially lower than that (K_s) of the crystalline matrix will result in a modest reduction of the modulus for the drained regime given by

$$K \sim K_s[1 - (K_s/K_f)\phi] \qquad [77]$$

(O'Connell and Budiansky, 1974; Hudson, 1981). In response to externally imposed changes in mean stress (**Figure 7**), fluid inclusions of common aspect ratio but different orientation experience the same perturbation in pore pressure – meaning that there is no distinction between the saturated isolated and isobaric regimes. Given the existence of a distribution of fluid-inclusion aspect ratios $p(\alpha)$, however, stress-induced fluid flow will occur, for example, between cracks and pores, with associated partial relaxation of the bulk modulus (Budiansky and O'Connell, 1980; **Figure 7**). In a partially molten medium, the maintenance of equilibrium proportions of the coexisting crystalline and liquid phases results in a lower effective compressibility for the fluid

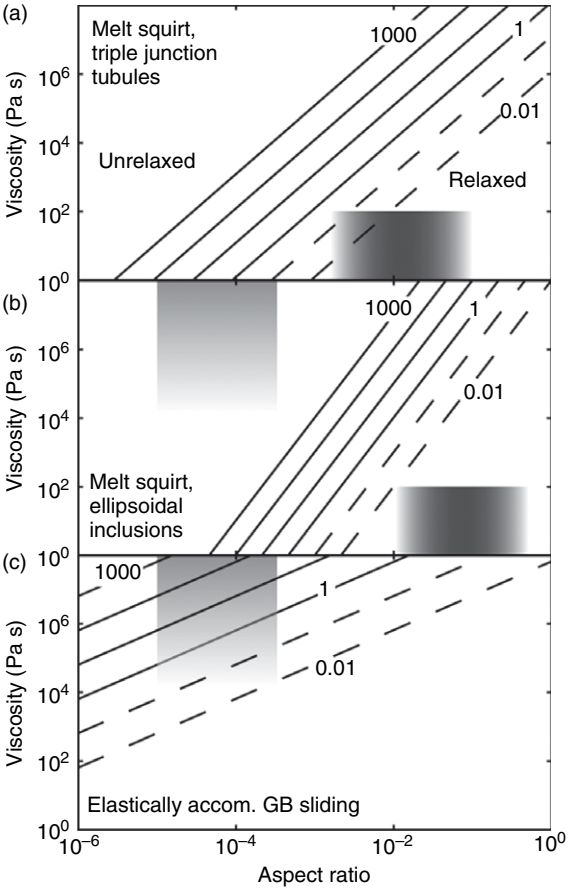

Figure 8 Relaxation times for elastically accommodated grain-boundary sliding and melt squirt as functions of the aspect ratio of the melt inclusion or grain-boundary region and of the melt or grain-boundary viscosity as described in the text. Values of the relevant elastic moduli, viscosities, and aspect ratios are appropriate for olivine-basalt system at 1200–1300°C. After Schmeling (1985), from Faul *et al.* (2004) with permission.

phase on sufficiently long timescales, and a large anelastic reduction in the bulk modulus as discussed in the previous section.

2.17.3 Insights from Laboratory Studies of Geological Materials

2.17.3.1 Dislocation Relaxation

2.17.3.1.1 Linearity and recoverability

Linearity of dislocation-controlled mechanical behavior requires that the dislocation density be independent of the applied stress and therefore that dislocation multiplication be avoided. For synthetic polycrystals of representative grain size $(1–100)\times10^{-6}$ m and Burgers vector of 5×10^{-10} m, the critical elastic strain amplitudes for the onset of Frank–Read multiplication of the longest possible dislocation segments (with $L=d$), calculated from eqn [13], are 5×10^{-4} to 5×10^{-6}, respectively. These correspond (for $G=50$ GPa) to stresses of 25–0.25 MPa, respectively. The linear regime is thus experimentally accessible over a wider range of stress and strain amplitudes in more fine-grained polycrystals (e.g., Gribb and Cooper, 1998a). The same argument applied to the larger grain sizes (1–10 mm) of the Earth's upper mantle yields critical elastic strain amplitudes of 5×10^{-7} to 5×10^{-8} for the onset of dislocation multiplication and hence nonlinear behavior. Of course, the presence of impurities and other dislocations means that dislocation segments will generally be substantially smaller than the grain size – expanding the field for linear behaviour to larger strains.

Recoverability of the nonelastic strains associated with dislocation migration requires that dislocations remain firmly pinned by impurities or interactions with other dislocations. For a scenario ($E_{up}\sim200–400$ kJ mol^{-1}, $a\sim b\sim5\times10^{-10}$ m and $L\sim(3–30)\times10^{-6}$ m) representative of silicate materials under laboratory or upper-mantle conditions, the critical stress for unpinning σ_{up} is predicted (eqn [51]) to be of order 0.1–1 MPa corresponding to shear strain amplitudes of order 10^{-6}–10^{-5}. It follows that thermally assisted unpinning is likely to be encountered in laboratory internal friction experiments typically performed at strain amplitudes of 10^{-6}–10^{-4} (e.g., Nowick and Berry, 1972; Karato and Spetzler, 1990). Under these circumstances, one would expect more strongly frequency-dependent attenuation ($Q^{-1}\sim\omega^{-1}$ in the viscous regime; **Figure 2**) and possibly nonlinear behavior resulting from dislocation multiplication in the longer dislocation segments. Unpinning is less likely at the lower stresses and strains of teleseismic wave propagation ($<10^{-6}$, e. g., Shearer, 1999, p.19).

2.17.3.1.2 Laboratory measurements on single crystals and coarse-grained rocks

Notwithstanding the potential importance of dislocation relaxation mechanisms in seismic wave attenuation, relevant laboratory experiments on geological materials have been few and far between. Gueguen *et al.* (1989) tested both untreated and predeformed single crystals of forsterite in low-strain (10^{-6}–10^{-5}) torsional forced oscillation at periods of $10^{-3.5}$–10 Hz and temperatures as high as 1400°C. The prior deformation was a compressive test at 1600°C to 1% strain with the maximum principal stress (20 MPa) oriented parallel to $[111]_c$, which direction later served also as the orientation of the torsional axis. The effect of the prior deformation was to substantially increase the average dislocation density from $\sim10^9$ to $\sim10^{11}$ m^{-2}. For each specimen the observed dissipation was dominated by an intense and broad absorption band (eqn [49]) with an activation energy $E=440\pm50$ kJ mol^{-1} and exponent $\alpha=0.20\pm0.03$. A minor absorption peak superimposed upon the background was observed near 0.1 Hz. The dissipation increased markedly as the result of prior deformation, about fourfold at 1400° and 1000 s period. Gueguen *et al.* argued plausibly that this observation, along with the similar activation energy for high-temperature dislocation creep in the same material, implicates relaxation associated with the stress-induced migration of the dominant $b=[100]$ edge dislocations. The similarly high activation energies for dislocation damping and creep have subsequently been interpreted by Karato (1998) to suggest a common reliance on the nucleation and migration of kink pairs (see below).

Torsional forced-oscillation measurements, performed at low strain amplitudes ($\sim10^{-6}$) and high temperatures (to 1500 K) on single-crystal MgO with an average dislocation density of about 5×10^9 m^{-2}, are similarly well described by eqn [49] with $E=230$ kJ mol^{-1} and $\alpha=0.30$ (Getting *et al.*, 1997). The much lower activation energy for dislocation damping than for dislocation creep (400 kJ mol^{-1}; Hensler and Cullen, 1968) led Karato (1998) to suggest that geometrical kink migration might account for the dislocation damping with nucleation and migration of kink pairs responsible for the dislocation creep.

Absorption-band behavior probably attributable at least in part to dislocation damping also dominates the high-temperature internal friction measured on relatively coarse-grained rocks (Berckhemer *et al.*, 1982; Kampfmann and Berckhemer, 1985; Jackson *et al.*, 1992). Activation energies for dissipation are generally comparable to those for creep – consistent with Karato's interpretation of the Gueguen *et al.* data for single-crystal forsterite. None of these studies involved a systematic examination of dislocation microstructure, and the shear moduli measured (at ambient pressure) in Berckhemer's laboratory were significantly compromised by thermal microcracking.

2.17.3.2 Stress-Induced Migration of Transformational Twin Boundaries in Ferroelastic Perovskites

Harrison and his colleagues have reported the results of a thorough study of the anelastic behavior associated with the stress-induced motion of domain walls in single crystals of the ferroelastic perovskite $LaAlO_3$ (Harrison and Redfern, 2002; Harrison *et al.*, 2004). They combined three-point bending experiments performed under combined steady and oscillating load with *in situ* optical observations of the domain wall motions. Essentially elastic behavior was observed for temperatures $T > T_c$ within the stability field of the high-symmetry phase (T_c is the phase transformation temperature). Strongly anelastic behavior, observed within the stability field of the low-symmetry ferroelastic phase, is associated with the thermally activated motion of the domain walls separating transformational twins formed spontaneously on cooling below T_c. At sufficiently low temperatures, domain-wall mobility is reduced to such an extent that the domain microstructure is frozen and elastic behavior with a high unrelaxed modulus prevails. The transition between the frozen and ferroelastic regimes is associated with pronounced relaxation ($\delta Y/Y \sim 0.9$) of Young modulus Y and an associated dissipation peak of amplitude ($\tan\delta = Q^{-1} \sim 1$). The dissipation peak is somewhat broader than the Debye peak of the standard anelastic solid and was modeled by Harrison and Redfern (2002) with a Gaussian distribution of activation energies suggestive of pinning of domain walls by oxygen vacancies. Subsequent studies on a number of additional ferroelastic perovskites have shown that appreciable domain wall mobility and associated anelastic relaxation may be restricted to phases with positive volume strain relative to the cubic parent and thick domain walls (Daraktchiev *et al.*, 2006). A broad dissipation peak newly recognized in previously published torsional forced-oscillation data for polycrystalline $CaTiO_3$ perovskite, is potentially attributable to the motion of twin domain boundaries. However, the $CaTiO_3$ peak is more probably associated with the rounding of grain edges at triple-junction tubules containing silicate impurity as argued in the following section.

2.17.3.3 Grain-Boundary Relaxation Processes

2.17.3.3.1 Grain-boundary migration in b.c.c. and f.c.c. Fe?

Like many other metals, the low-temperature body-centered cubic (b.c.c.) polymorph of iron was studied with resonant (pendulum) techniques in the early days of internal friction studies. More recently, Jackson *et al.* (2000) employed subresonant forced-oscillation methods to probe the viscoelastic behavior of mildly impure polycrystalline iron over an extended temperature range reaching well into the stability field of the high-temperature f.c.c. phase.

Markedly viscoelastic behavior, dominated by the monotonically frequency and temperature-dependent 'high-temperature background', was observed within each of the b.c.c. and f.c.c. stability fields for both mild steel and soft iron compositions. The behavior of the b.c.c. phase is adequately described by eqn [49] with an activation energy of $E = 280(30)$ kJ mol^{-1} not very different from that for lattice diffusion (239 kJ mol^{-1}; Frost and Ashby, 1982) and $\alpha = 0.20(2)$. For the f.c.c. phase, α determined during staged cooling from 1300°C to 800°C typically assumes values of 0.2–0.3 at the highest and lowest temperatures within this range but reaches significantly lower values ~0.1 at intermediate temperatures. The result is a poorly defined Q^{-1} plateau at short periods and 900–1100°C, suggestive of a broad Q^{-1} peak superimposed upon the background (Jackson *et al.*, 2000, figure 8b).

Each of these phases displays unusually strong elastic anisotropy at elevated temperatures and ambient pressure: G_{RS}/G_{HS} decreasing from 0.91 to 0.61 between 20°C and 900°C for b.c.c.-Fe (Dever, 1972), whereas the only available single-crystal elasticity data for f.c.c.-Fe yield $G_{RS}/G_{HS} = 0.74(1)$ at 1155°C. Relaxation of the initially inhomogeneous stress field toward the Reuss state of uniform stress by grain-boundary migration, first suggested by Leak (1961), is accordingly a potentially important relaxation

mechanism in polycrystalline iron prompting more detailed investigation now in progress.

2.17.3.3.2 Grain-boundary sliding

The high-temperature behavior of fine-grained synthetic rocks (and analogous ceramic materials) has been the focus of a substantial body of recent work. Fine-grained ultramafic materials with and without a small melt fraction have been made by hot-isostatic pressing of powders prepared by crushing natural dunites or olivine crystal separates, or by a solution–gelation procedure (Tan *et al.*, 1997, 2001; Gribb and Cooper, 1998a, 2000; Jackson *et al.*, 2002, 2004; Xu *et al.*, 2004). These studies have consistently revealed broad absorption-band behavior; superimposed dissipation peaks were reported only in the studies of Jackson *et al.* (2004) and Xu *et al.* (2004) of melt-bearing materials.

Of these materials, only the olivine polycrystals, prepared from hand-picked natural olivine crystals or sol–gel precursors, are pure enough to remain genuinely melt free during testing by high-temperature mechanical spectroscopy (Jackson *et al.*, 2002; see also Jackson *et al.* (2004)). The reconstituted dunite tested by Gribb and Cooper (1998a) is only nominally melt free – the usual inventory of impurities being expected to produce 0.1–1% melt at temperatures of 1200–1300°C. Accordingly, it is the study by Jackson *et al.* (2002, 2004) that defines the base-line behavior of genuinely melt-free polycrystalline olivine. The results depart markedly from the prescriptions of the widely used Raj–Ashby model of elastically and diffusionally accommodated grain-boundary sliding. First, despite intensive sampling of the transition from elastic behavior through essentially anelastic into substantially viscous deformation, dissipation peaks attributable to elastically accommodated grain-boundary sliding are conspicuous by their absence. Instead, the dissipation increases monotonically with increasing oscillation period and temperature (**Figure 9(a)**) in the manner of the high-temperature background. Second, the variation with oscillation period and grain size, given by $Q^{-1} \sim (T_o/d)^{1/4}$, is much milder than predicted for the diffusional creep transient (eqn [62]). For other ceramic systems lacking a widely distributed grain-boundary phase of low viscosity, 'grain-boundary' Q^{-1} peaks are similarly absent or very broad and of subsidiary significance relative to the background dissipation (Pezzotti *et al.*, 1998; Lakki *et al.*, 1999; Webb *et al.*, 1999). Third, complementary microcreep tests on the same olivine materials clearly demonstrate a continuous transition from elastic through anelastic to viscous behavior, implying that the timescales τ_e and τ_d given by eqns [60] and [61] above are not as widely separated as suggested by the Raj–Ashby theory (Jackson *et al.*, 2002).

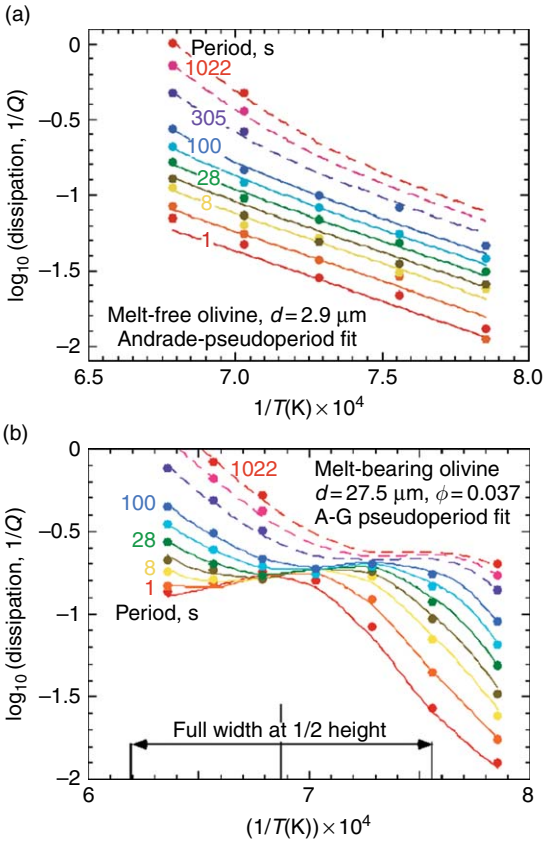

Figure 9 Representative data displaying contrasting variations of dissipation with oscillation period and temperature (a) monotonic absorption-band behavior for a genuinely melt-free polycrystalline olivine, the curves representing an Andrade-pseudoperiod fit to the Q^{-1} data. (b) A broad dissipation peak superimposed upon the monotonic background for a melt-bearing olivine polycrystal, the curves representing an Andrade–Gaussian pseudoperiod fit to Q^{-1} data. (a and b) Adapted from Jackson I, Faul UH, Fitz Gerald J, and Morris SJS (2006) Contrasting viscoelastic behaviour of melt-free and melt-bearing olivine: Implications for the nature of grain-boundary sliding. *Materials Science and Engineering A* 442: 170–174.

In the presence of small basaltic melt fractions ranging from 10^{-4} to 4×10^{-2}, qualitatively different behavior has been observed in the form of a broad dissipation peak superimposed upon a dissipation background enhanced relative to that for melt-free material of the same grain size (Jackson *et al.*, 2004; **Figure 9(b)**). The peak width exceeds that of the Debye peak of the standard anelastic solid by about two decades in period and is independent of temperature but varies mildly with the breadth of the grain-size distribution. The peak height is well

described by power-law dependence upon maximum melt fraction. The peak position (period) varies exponentially with $1/T$ (with a high activation energy E_P of 720 kJ mol^{-1} – possibly reflecting both thermal and compositional influences upon viscosity) and linearly with grain size. This grain-size sensitivity is that expected of elastically accommodated grain-boundary sliding (eqn [60]). These observations have been compared and contrasted with the somewhat different findings of Gribb and Cooper (2000) and Xu *et al.* (2004) by Faul *et al.* (2004).

It has long been understood that the viscoelastic relaxation associated with partial melting should depend upon the extent to which the melt wets the grain boundaries (e.g., Stocker and Gordon, 1975). It is well known that basaltic melt in textural equilibrium does not normally wet olivine grain faces – being confined instead to a network of interconnected grain-edge tubules of cuspate triangular cross-section along with a population of larger localized melt pockets (Faul *et al.*, 1994). Among the melt-bearing olivine polycrystals described by Faul *et al.* (2004), for example, the melt fraction ranges widely from $\sim 10^{-4}$ to 4×10^{-2} with aspect ratios of 3×10^{-3} to 10^{-1} for grain-edge tubules and 10^{-2} to 5×10^{-1} for the isolated melt pockets. For such aspect ratios and the bulk melt viscosities of 1–100 Pa s appropriate for 1200–1300°C, melt squirt, whether between adjacent tubules or between adjacent melt pockets is expected at timescales substantially shorter than seismic periods (**Figure 8(a)** and **8(b)**) in accord with the results of previous analyses (Schmeling, 1985; Hammond and Humphreys, 2000a). Moreover, the relaxation strength for squirt flow between melt tubules is low (Mavko, 1980): ~0.02 corresponding to a Q^{-1} peak height of only 0.01 for a melt fraction ϕ of 0.04. For these and other reasons given by Faul *et al.* (2004), melt squirt was rejected as a viable explanation for the melt-related dissipation peak. Instead, it was recognized that elastically accommodated grain-boundary sliding involving boundary regions of aspect ratio $\sim 10^{-4}$ has the potential to contribute to attenuation at seismic frequencies – provided that the effective grain-boundary viscosity is, not unreasonably, 10^4–10^9 Pa s for temperatures of 1300–1000°C (**Figure 8(c)**).

It remained to explain the absence of a Q^{-1} peak associated with elastically accommodated grain-boundary sliding in the genuinely melt-free materials. The key microstructural difference that appears to correlate with the presence or absence of a dissipation peak in these materials is the rounding of olivine grain edges at the triple-junction tubules of the melt-bearing specimens (**Figure 10**). In contrast, the tight grain-edge interlocking characteristic of melt-free material (**Figure 10**) apparently inhibits elastically accommodated sliding – a conclusion supported by the foregoing discussion (following eqn [59]) of the Raj and Ashby model. A corollary of this interpretation is that the background dissipation in both classes of material would be attributed to diffusionally accommodated grain-boundary sliding. Thus for the melt-bearing materials, it is suggested that grain-boundary sliding occurs with concurrent elastic and diffusional accommodation.

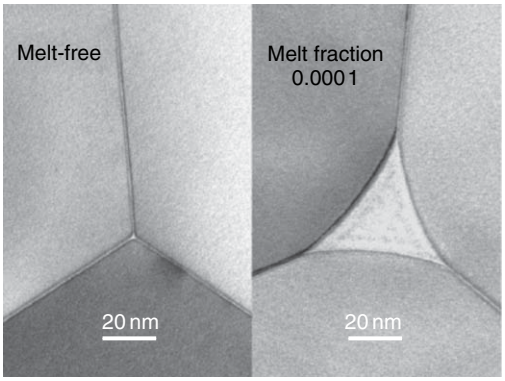

Figure 10 Contrasting grain-edge microstructures in melt-free and melt-bearing olivine polycrystals. For the melt-free material, olivine grain edges are tightly interlocking, whereas the presence of grain-edge melt tubules results in a significant radius on each olivine grain edge. These microstructural differences are considered responsible for the qualitatively different dissipation behaviors highlighted in **Figure 9**. Adapted from Faul UH, Fitz Gerald JD, and Jackson I (2004) Shear-wave attenuation and dispersion in melt-bearing olivine polycrystals. Part II: Microstructural interpretation and seismological implications. *Journal of Geophysical Research* 109: B06202 (doi:10.1029/2003JB002407).

Broadly similar observations have recently been made for polycrystalline MgO. Dense polycrystals of high purity display only a monotonically frequency and temperature-dependent Q^{-1} background and associated dispersion of the shear modulus (Barnhoorn *et al.*, 2006). In marked contrast, a previous study of MgO of lower purity (Webb and Jackson, 2003) revealed a pronounced dissipation peak, superimposed upon the background, and now attributed to elastically accommodated grain-boundary sliding facilitated by the presence of a grain-boundary phase of low viscosity.

Further examples of both types of high-temperature viscoelastic behavior are provided by the fine-grained polycrystalline titanate perovskites studied as analogues for the high-pressure silicate perovskites by

Webb *et al.* (1999). The purest and microstructurally simplest of these specimens was an $SrTiO_3$ specimen of 5 μm grain size. Its grains are untwinned and its essentially impurity-free grain boundaries meet in grain edge triple-junctions invariably less than 20 nm in cross-sectional dimension. The lack of an extensive network of substantial grain-edge triple-junction tubules is reflected in background-only dissipation generally well described for temperatures between 900°C and 1300°C by eqn [49]. On the other hand, the $CaTiO_3$ specimens of 3 and 20 μm grain size are pervasively twinned and contain a significant level of silicate impurity responsible for well-developed networks of grain-edge tubules of triangular-cuspate cross-section. With the benefit of hindsight, deviations from power-law fits to the $Q^{-1}(T_o)$ data at 1000°C and 1050°C (Webb *et al.*, 1999, table 4 and figure 13) for the 20 μm specimen are consistent with the presence of a broad dissipation peak analogous to those characteristic of melt-bearing olivine. For the more fine-grained $CaTiO_3$ specimen, any such peak may be masked by the relatively low-temperature onset of markedly viscous behavior.

The growing body of experimental observations thus indicates that the transition from elastic through anelastic to viscous behavior in fine-grained geological (and ceramic) materials is not satisfactorily described by the classic Raj–Ashby theory. In particular,

1. sufficiently pure materials display no high-temperature dissipation peak attributable to elastically accommodated grain-boundary sliding;
2. low grain-boundary viscosity is a necessary but not sufficient condition for elastically accommodated sliding: rounding of grain edges at triple junctions is also required; and
3. diffusional accommodation of grain-boundary sliding, presumably responsible for the ubiquitous high-temperature background with its mildly and monotonically frequency-dependent dissipation, can occur without or alongside elastic accommodation (Barnhoorn *et al.*, 2006).

These observations have provided the motivation for a new approach to the micromechanical modeling of grain-boundary sliding free from the principal limitations of Raj–Ashby theory as discussed in Section 2.17.2.

2.17.3.4 Viscoelastic Relaxation in Cracked and Water-Saturated Crystalline Rocks

The sparse experimental observations concerning the effect of water saturation on the elastic moduli of cracked crystalline rocks of relatively low-porosity, recently assembled by Lu and Jackson (2006), are reproduced in **Figure 11**. The existence of a mechanical relaxation spectrum first suggested by Gordon (1974) is confirmed by this more recent compilation. Ultrasonic, resonance and forced-oscillation methods together provide access to more than eight decades of period or frequency. The fractional change in elastic wave speed $\delta V_i/V_i$ that results from water saturation (with $P_f = 0$) is plotted for the compressional (i = P), shear (i = S), and extensional (i = Y) bar modes. For μs–ms periods, the wave speeds are consistently increased by water saturation, the effect being more pronounced for compressional and extensional modes than in shear. The sign is reversed for periods greater than ~0.1 s with significant negative perturbations to both extensional and shear wave speeds for the 10–100 s periods of forced-oscillation methods.

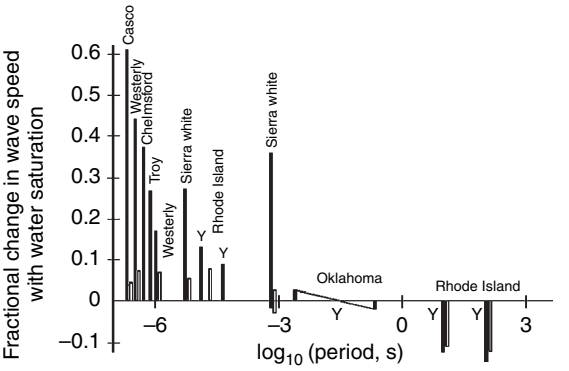

Figure 11 The effect of water saturation of granite (with zero pressure and confining pressure) on the speed of compressional (unlabeled solid bars), bar-mode longitudinal (solid bars labeled 'Y'), and shear waves (unfilled bars). The sources of the data for the various granite specimens (named after their provenance) are given by Lu and Jackson (2006, figure 11) – after which this figure has been redrawn.

Interpretation of the broad trend evident in **Figure 11** requires estimates of the characteristic times for the various fluid-related relaxation mechanisms discussed in Section 2.17.2, for the special case of water saturation of cracks of aspect ratio $\sim 10^{-3}$. For relaxation of shear stress within an individual grain-scale fluid inclusion (eqn [71]), $\tau_e \sim \eta_f / G_u \alpha \sim 10^{-11}$ s; for squirt between adjacent cracks (eqn [73]), $\tau_{s,e} = 2\pi\eta_f / K_s \alpha_e{}^3 \sim 10^{-4}$ s; and for the draining of a cm-sized laboratory rock specimen of porosity $\phi \sim 0.01$ and permeability $\sim 10^{-18}$ m^2, $\tau_{dr} = \eta_f \phi R^2 / k K_f \sim 10^{-1}$ s (Lu and Jackson, 2006). Accordingly, Lu and Jackson (2006) concluded that

the ultrasonic measurements at periods $<10^{-5}$ s probe the saturated isolated regime, whereas near-zero values of $\delta G/G$, and hence $\delta V_S/V_S$, at the ms periods of resonance techniques are characteristic of the saturated isobaric regime. Near-zero values of $\delta K/K$ for periods $>10^{-3}$ s are indicative of the drained regime. Chemical effects of water saturation, such as increased crack density and reduction in the stiffness of grain contacts, are required to explain the negative values of $\delta V/V$ in experimental data obtained at periods greater than 0.01 s (Lu and Jackson, 2006).

2.17.4 Geophysical Implications

2.17.4.1 Dislocation Relaxation

2.17.4.1.1 Vibrating string model

The possibility that viscoelastic relaxation associated with the stress-induced motion of dislocations might explain the attenuation and dispersion of seismic waves, especially in the Earth's upper mantle, has been widely canvassed (Gueguen and Mercier, 1973; Minster and Anderson, 1981; Karato and Spetzler, 1990; Karato, 1998). Gueguen and Mercier (1973) invoked the vibrating string model of dislocation motion as an explanation for the upper-mantle zone of low wave speeds and high attenuation. They associated an intragranular dislocation network with any observable high-temperature relaxation peak and suggested that a grain-boundary network of more closely spaced dislocations might explain the high-temperature background attenuation. It was suggested that impurity control of dislocation mobility might yield relaxation times appropriate for the seismic-frequency band.

A more ambitious attempt to produce a model of dislocation-controlled rheology consistent with both seismic-wave attenuation and the long-term deformation of the mantle was made by Minster and Anderson (1981). They envisaged a microstructure established by dislocation creep in response to the prevailing tectonic stress σ_t and comprising subgrains of dimension $\underline{L}$

$$\underline{L} = \gamma_s Gb/\sigma_t = \gamma_s L_c \qquad [78]$$

with a mobile dislocation density

$$\Lambda_m = \gamma(\sigma_t/Gb)^2 = \gamma L_c^{-2} \qquad [79]$$

where $L_c = Gb/\sigma_t$ is the critical dislocation link length for multiplication by the Frank–Read mechanism (see discussion following eqn [12]). From laboratory experiments on olivine (Durham *et al.*, 1977), it was estimated that $\gamma_s \sim 20$ for well-annealed mantle olivine; γ is a constant of order unity (Frost and Ashby, 1982). Furthermore, it was argued that the distribution of dislocation segment lengths will be dominated by those of length

$$L \sim (5/3)L_c \qquad [80]$$

for which the dislocation multiplication time, calculated with a migration velocity given by eqn [14], is a minimum. It follows from eqns [78]–[80] that the dislocation density within the subgrains is essentially that (L^{-2}) of the Frank network with dislocation relaxation strength $\Delta \sim 0.1$ (eqn [23]). For $\sigma_t \sim 1$ MPa (strain rate of 10^{-15} s^{-1} with effective viscosity of 10^{21} Pa s), $L_c \sim 30 \times 10^{-6}$ m and $\Lambda_m \sim 10^9$ m^{-2}. It was suggested that the total dislocation density should be much higher – being dominated by dislocations organised into the subgrain walls. The climb-controlled motion of these latter dislocations was invoked to explain deformation at tectonic stresses and timescales (Minster and Anderson, 1981).

Their suggestion of a dominant link length disallows an absorption band based on a wide distribution of segment lengths (eqn [50]). Minster and Anderson (1981) suggested instead that the seismic absorption band reflects a spectrum of activation energies. A frequency-independent upper-mantle Q^{-1} of 0.025 was shown to require a range δE of about 80 kJ mol^{-1} and to produce an absorption band only two to three decades wide.

A unified dislocation-based model for both seismic wave attenuation and the tectonic deformation of the Earth's mantle has been sought more recently by Karato and Spetzler (1990) and Karato (1998). Karato and Spetzler (1990) emphasized the apparent paradox whereby a Maxwell model based on reasonable steady-state viscosities seriously underestimates the level of seismic-wave attenuation (their figure 3). Equally, a transient-creep description of seismic-wave attenuation extrapolated to tectonic timescales (Jeffreys, 1976) seriously overestimates the mantle viscosity. For a unified dislocation-based model, it is thus required that dislocations have much greater mobility (velocity/stress) at seismic frequencies than for tectonic timescales. Karato and Spetzler's assessment of relaxation strengths and relaxation times, based on the vibrating-string model of dislocation motion (eqn [23]) and revisited with a somewhat higher dislocation density of 10^9 m^{-2} (eqn [79] applied to the upper mantle as above) is in general accord with that of Minster and Anderson. In particular, reasonable

levels of seismic wave attenuation ($10^{-1} > \Delta > 10^{-3}$) would require segment lengths L of $(1–10) \times 10^{-6}$ m, and a specific range of dislocation mobilities (b/B in eqn [14]) would be needed for relaxation times in the seismic band (Karato and Spetzler, 1990, figure 7). The issue in all such analyses is to relate key parameters controlling Δ, τ, and indeed the steady-state effective viscosity η, to the intrinsic and/or extrinsic properties of dislocations, as appropriate. Karato and Spetzler noted that dislocation mobility is expected to increase with increasing temperature and water content but to decrease with increasing pressure. The segment length L for the vibrating string model was shown to depend in different ways on the tectonic stress according to whether pinning is effected by interaction with impurities or other dislocations.

2.17.4.1.2 Kink model

The feasibility of seismic-wave attenuation resulting from the stress-induced migration of kinks was also briefly explored by Karato and Spetzler (1990) and analyzed in more detail by Karato (1998). In the latter study, Karato identified three distinct stages of dislocation relaxation to be expected with progressively increasing temperature or stress and/or decreasing frequency. Stage I involves the reversible migration of pre-existing geometrical kinks along Peierls valleys with characteristic timescale and relaxation strength given by eqns [27] and [28] above. The maximum anelastic strain resulting from migration of geometrical kinks (eqn [30]) is of order 10^{-6} for a Frank network of dislocations with $\Lambda \sim L^{-2} \sim 10^{9}\,\mathrm{m}^{-2}$ – consistent with the large relaxation strength for this mechanism (eqn [28]).

Stage II is associated with the spontaneous nucleation of isolated kink pairs followed by the separation of the newly formed kinks of opposite sign. The resulting anelastic relaxation, usually associated with the Bordoni dissipation peak for deformed metals (e.g., Seeger, 1981; Fantozzi *et al.*, 1982), is described in detail by Seeger's theory outlined above and culminating in eqns [43]–[45]. At the still higher temperatures/larger stresses of stage III, it was envisaged by Karato that continuous nucleation and migration of kinks, possibly enhanced by unpinning of dislocations, would allow the arbitrarily large, irrecoverable strains of viscous behavior.

The relaxation times expected for geometrical kink migration and kink-pair formation and migration in the Earth's upper mantle were shown by Karato (1998) to be broadly compatible with strain–energy dissipation at teleseismic and lower frequencies. It was thus concluded that attenuation and associated dispersion, microcreep, and large-strain creep possibly share a common origin in dislocation glide. The results of such calculations, repeated with eqns [27] and [28] and [43]–[45] above, are presented in **Figure 12**. For this purpose we have used $a_d \sim b \sim a \sim 5 \times 10^{-10}$ m, $G_u = 60$ GPa, $v_{k0} \exp(S_m/k) \sim 10^{13}$ Hz (Seeger and Wüthrich, 1976), and have chosen a relatively large value of $H_m = 200\,\mathrm{kJ\,mol^{-1}}$ intended to reflect kink interaction with impurities and $\sigma_P/G = 0.01$ which, through eqn [39], fixes H_k at $162\,\mathrm{kJ\,mol^{-1}}$ (so that $2H_k + H_m$ is of order $500\,\mathrm{kJ\,mol^{-1}}$: c.f. Karato, 1998, figure 3). Substantially larger values of σ_P/G have been suggested (Frost and Ashby, 1982, p. 106; Karato and Spetzler, 1990, p. 407), but when combined with Seeger's theory yield implausibly high kink formation energies. Relaxation times have been calculated for indicative lengths of 1 and 100 μm for dislocation segments. The results of these calculations (**Figure 12**), like those of Karato (1998), indicate that the migration of geometrical kinks could result in anelastic relaxation within the seismic frequency band at typical upper-mantle temperatures. The much higher activation energy for the formation and

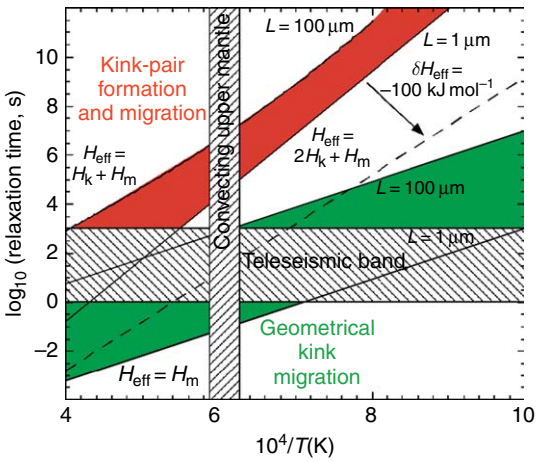

Figure 12 Computed relaxation times for Seeger's (1981) kink model of dislocation mobility. The green band represents relaxation associated with the migration of geometrical kinks with segment lengths of $(1–100) \times 10^{-6}$ m and an activation energy for kink migration $H_m = 200\,\mathrm{kJ\,mol^{-1}}$. Relaxation times calculated from eqns [36]–[39] for the formation and migration of kink pairs are indicated by the red band for the same range of segment lengths and an activation energy for the formation of a single kink of $162\,\mathrm{kJ\,mol^{-1}}$ corresponding through Seeger's (1981) theory with $\sigma_P/G = 0.01$. The effect of an effective activation energy lower by $100\,\mathrm{kJ\,mol^{-1}}$ is shown by the broken line.

migration of kink pairs (here $2H_k + H_m = 524\,\mathrm{kJ\,mol^{-1}}$) results in much longer relaxation times – ranging from $\sim 10^4$ to $10^{6.5}$ s at the highest plausible upper-mantle temperatures ~1700 K. An effective activation energy lower by about $100\,\mathrm{kJ\,mol^{-1}}$ would be required to bring the relaxation involving kink-pair formation and migration into substantial overlap with the seismic frequency band for typical temperatures of the convecting upper mantle as indicated by the broken line in **Figure 12**. Alternatively, kink-pair formation and migration might result in relaxation at the day-to-month timescales of Earth tides. Similarly, high activation energies for attenuation and creep in olivine are interpreted by Karato (1998) to imply the need for kink nucleation for both processes, whereas the low reported activation energy for attenuation in single-crystal MgO might reflect a dominant role for the migration of geometrical kinks.

2.17.4.2 Grain-Boundary Processes

Gribb and Cooper (1998a) explained their observations of high-temperature absorption band behavior (eqn [49] with $\alpha \sim 0.35$) for a reconstituted dunite of 3 μm grain size in terms of the transient diffusional creep modeled by Raj (1975). The strong $Q^{-1} \sim d^{-1}$ grain-size sensitivity implied by this model (eqn [62]) extrapolated to mm–cm grain size seriously underestimates upper-mantle seismic wave attenuation. Gribb and Cooper (1998a) sought to resolve this discrepancy by invoking diffusionally accommodated sliding on subgrain boundaries rather than grain boundaries. It was suggested that this mechanism could also reconcile the Gribb and Cooper data with those of Gueguen *et al.* (1989) for pre-deformed single-crystal forsterite. The increased attenuation resulting from prior deformation has been more naturally interpreted by others (including Gueguen *et al.* (1989)) as prima facie evidence of dislocation relaxation as discussed above.

The milder grain-size sensitivity $Q^{-1} \sim d^{-1/4}$ subsequently directly measured by Jackson *et al.* (2002) for melt-free polycrystalline olivine yields extrapolated levels of attenuation for mantle grain sizes more consistent with seismological observations. More recently, Faul and Jackson (2005) have employed a generalized Burgers model (eqns [8]) to provide an internally consistent description of the variations of both shear modulus and dissipation with frequency, temperature, and grain size for melt-free polycrystalline olivine. Extrapolation (principally in grain size) of this model to upper-mantle conditions provides a satisfactory first-order explanation for much of the variability of seismic wave speeds and attenuation in the upper mantle. The presence of a zone of low shear wave speeds and high attenuation in the oceanic upper mantle and its systematic variation with age of the overlying lithosphere can be explained by lateral temperature variations without recourse to more exotic explanations such as water or partial melting (Anderson and Sammis, 1970; Karato and Jung, 1998). Beneath the continents, lateral variations in seismic structure can be explained by variations in the depth at which the conductive part of the geotherm intersects a common mantle adiabat.

In more active tectonic provinces such as mid-ocean ridges, subduction zones, and back-arc basins, partial melting is expected to influence the wave speeds and attenuation. Superposition of the experimentally observed melt-related dissipation peak upon a melt-enhanced background, extrapolated to upper-mantle conditions, results in generally higher but less markedly frequency-dependent attenuation than for melt-free material under otherwise similar conditions (Faul *et al.*, 2004, figure 13).

2.17.4.3 The Role of Water in Seismic Wave Dispersion and Attenuation

The crystalline rocks of the Earth's upper crust are commonly pervasively cracked and often water-saturated. The sparse laboratory measurements so far performed on cracked and water-saturated low-porosity rocks are strongly suggestive of intense viscoelastic relaxation (Section 2.17.3). The inference is that modulus relaxation and strain–energy dissipation, associated with stress-induced fluid flow on various spatial scales, are to be expected for frequencies ranging from ultrasonic (MHz) to teleseismic (mHz–Hz). It follows that conventional (ultrasonic) measurements will tend to overestimate seismic wave speeds (especially V_P) and hence also the ratio V_P/V_S. Accordingly, high-frequency (ultrasonic) laboratory data cannot be applied directly in modeling the wave speeds and attenuation in fluid-saturated crustal rocks. Rather, it would be expected from the analysis of Sections 2.17.2 and 2.17.3 that the shear modulus of water-saturated rock at teleseismic frequencies should be comparable with that of the dry rock. Contrasting behavior is expected for the bulk modulus of the cracked rock – which for undrained conditions will be significantly increased by water saturation (eqn [77]).

In the deeper crust and mantle, free water will typically have a more transient existence, but a small amount of water dissolved in a major nominally anhydrous mineral (like olivine or pyroxene) has the potential to significantly enhance solid-state viscoelastic relaxation, for example, by increasing the mobility of dislocations. There are as yet no directly relevant experimental data, but the potential has recently been demonstrated (Shito *et al.*, 2006) for future analyses in which observed variations in V_P, V_S, and Q^{-1} might be combined to map variations in chemical composition, temperature, and the water content of the upper mantle.

2.17.4.4 Bulk Attenuation in the Earth's Mantle

If pressure-induced changes in the proportions of coexisting crystalline phases were to result in relaxation of the bulk modulus within the seismic frequency band (for which there is little seismological evidence), conditions would be most favorable in the upper mantle and transition zone. It is here that relatively high temperatures facilitating rapid phase transformation are combined with phase transformations involving substantial density contrast. Consider, for example, the olivine–wadsleyite transformation with an *in situ* density contrast of ~6%. This is diluted in the pyrolite composition by an almost equal volume of the $(M, Al)(Si, Al)O_3$ (M = Mg, Fe) component playing an essentially passive role. However, the presence of the latter component and partitioning between it and the M_2SiO_4 phases reduces the width of the binary loop to $\delta P < 0.3$ GPa (Stixrude, 1997; Irifune and Isshiki, 1998; Weidner and Wang, 2000). Thus, eqn [66] for the relaxation strength yields $\Delta_v \sim (150\,\text{GPa}/0.3\,\text{GPa})(0.03) = 15$, but of course any resulting compressional wave attenuation would be confined to a layer of thickness ~10 km comparable with the seismic wavelength. For the wider two-phase loop of the pyroxene–garnet phase transformation, $\Delta_v \sim (150\,\text{GPa}/5\,\text{GPa})\ (0.03) = 0.9$, so that any seismic wave attenuation, although of lower intensity, would more readily observed. The large relaxation strengths for this process mean that it probably plays an important role somewhere in the Earth's wide mechanical relaxation spectrum. For the olivine–wadsleyite transformation, the relaxation time estimated from eqn [78] with D_{Si} in olivine at 1600 K (Brady, 1995) and $d = 10^{-2}$ m is

$$\tau(\text{s}) = 2 \times 10^{17} (p_s/\delta P)^2 = 2 \times 10^{17} \times (K\varepsilon_e/\delta P)^2 \sim 10^{23}\varepsilon_e^2 \quad [81]$$

or 10^5–10^9 s for a strain ε_e of 10^{-9}–10^{-7} suggesting the possibility of bulk relaxation at tidal and longer periods.

At the shorter periods of teleseismic waves, significant bulk dissipation Q_K^{-1} may arise from the elastic heterogeneity of aggregates of anisotropic mineral grains as explained in Section 2.17.3. Values of $Q_K^{-1}/Q_G^{-1} \sim 0.01$ were calculated for polycrystalline forsterite and a peridotitic composite, representative of upper-mantle materials by Budiansky and O'Connell (1980). For the mixture of silicate perovskite and magnesiowüstite that dominates the mineralogical makeup of the Earth's lower mantle, the relaxation of the bulk modulus is expected to decrease with increasing pressure along the high-temperature adiabat from ~2% at zero pressure to <1% in the deepest mantle (Heinz, *et al.*, 1982; Jackson, 1998). Thermoelastic relaxation (eqn [54]) may enhance the bulk dissipation that is the direct consequence of elastic heterogeneity, to levels sufficient to explain the modest amount of bulk dissipation evident in the damping of the low-order radial modes of free oscillation of the Earth (Budiansky *et al.*, 1983).

2.17.4.5 Migration of Transformational Twin Boundaries as a Relaxation Mechanism in the Lower Mantle?

It has been suggested by Harrison and Redfern (2002) that the mobile transformational twin boundaries that are clearly responsible for intense dissipation and associated modulus relaxation observed in the laboratory in some pervasively twinned perovskite crystals might also operate in the Earth's silicate perovskite-dominated lower mantle. Pinning of such domain walls by oxygen vacancies as in $LaAlO_3$ perovskite would result in anelastic relaxation times for lower-mantle conditions much shorter than teleseismic periods. Stronger pinning of domain walls by defects, impurities, and grain boundaries would be required for relaxation times within the seismic band (Harrison and Redfern, 2002). Indeed, pinning so effective as to eliminate significant anelastic relaxation has subsequently been observed in orthorhombic $(Ca, Sr)TiO_3$ perovskites (Daraktchiev *et al.*, 2006). More critically, however, substantially different microstructures are to be expected in the silicate perovskites of the lower mantle. The sustained operation of tectonic stress over geological

timescales should enlarge the domains of any transformational twins that are favorably oriented with respect to the ambient stress field resulting in a population of mainly single-domain grains and incidentally some degree of lattice preferred orientation. It therefore seems unlikely that transformational twinning will play a major role in seismic wave attenuation in the lower mantle.

2.17.4.6 Solid-State Viscoelastic Relaxation in the Earth's Inner Core

The combination of low (but finite) rigidity and marked attenuation that characterize the Earth's inner core have long been regarded as highly anomalous and have often been explained in terms of partial melting, as reviewed by Jackson *et al.* (2000; see also Vočadlo (2007)). However, the relatively low value of G/K and hence high Poisson's ratio ($v = 0.44$) are at least in part the expected consequence of the compression of a close-packed crystalline solid (Falzone and Stacey, 1980). First-principles calculations suggest values of ν 0.29–0.32 at inner core densities and 0 K (Vočadlo *et al.*, 2003a, table 1) and the possibility of a further substantial increase due to the usual anharmonic influence of temperature (Steinle-Neumann *et al.*, 2003; Vočadlo, 2007). Laboratory measurements reviewed above have revealed pronounced viscoelastic relaxation in both b.c.c. and f.c.c. phases of mildly impure iron at homologous temperatures (T/T_m) reaching 0.6 and 0.9, respectively (Jackson *et al.*, 2000). Given the high homologous temperature ($T/T_m \sim 1$) of the inner core, intense solid-state viscoelastic relaxation is inevitable. The experimental evidence for solid-state viscoelastic relaxation in iron would have direct relevance to the Earth's inner core if the b.c.c. phase were to be stabilized by high temperature and/or the accommodation of light alloying elements (Vočadlo *et al.*, 2003b; Vočadlo, 2007). The inevitable contribution of solid-state relaxation to the observed seismic wave attenuation ($Q^{-1}{}_G \sim 0.01$–0.02) and to any required viscoelastic relaxation of the shear modulus (~1.5% per decade of frequency for $Q^{-1} = 0.01$) must therefore be considered before partial melting is invoked (e.g., Vočadlo, 2007).

2.17.5 Summary and Outlook

This survey of viscoelastic relaxation mechanisms potentially relevant to the Earth's deep interior highlights the disparity in maturity between theory and experimental observations. Long-established theoretical models provide plausible, if highly idealized, descriptions of viscoelastic relaxation associated with dislocation motion and grain-boundary sliding. The stress-induced redistribution of an intergranular fluid is similarly well-described theoretically. That this substantial framework has not yet been more thoroughly tested against experimental observations is attributable in part to limitations in the experimental methods that have been overcome only relatively recently. The pioneering experimental work of the 1950s and 1960s focused on low-temperature internal friction peaks in metals investigated with resonant (i.e., pendulum) techniques. This isochronal approach has the major disadvantage that it provides no opportunity to observe the relaxation spectrum by continuous variation of frequency under isothermal conditions. More recently, there has been growing recognition of the superiority of mechanical spectroscopy methods in which subresonant forced oscillations probe the relaxation spectrum under isothermal high-temperature conditions affording the benefit of a stable microstructure (Woirgard *et al.*, 1981; Berckhemer *et al.*, 1982; Gadaud *et al.*, 1990; Jackson and Paterson, 1993; Getting *et al.*, 1997; Gribb and Cooper, 1998b; Schaller *et al.*, 2001). The latter technique is particularly well suited to investigation of the high-temperature background – the monotonic variation of Q^{-1} with frequency and temperature that typically dominates the dissipation at high temperature and low frequency. In addition, complementary microcreep tests are now being more widely used to distinguish between recoverable (anelastic) and permanent (viscous) strains.

Sustained application of these improved methods to well-characterized specimens of geological and ceramic materials is beginning to elucidate the microscopic processes responsible for their high-temperature viscoelastic relaxation. The consistent picture emerging from studies of fine-grained polycrystalline materials lacking a dispersed secondary phase of low viscosity is that of a broad absorption band (eqn [49]) involving mild frequency dependence of Q^{-1} and an Arrhenian variation with temperature with an activation energy often comparable with that for creep. The lack of a dissipation peak attributable to elastically accommodated grain-boundary sliding is difficult to reconcile with the classic Raj–Ashby model of the breakdown of elastic behavior – suggesting instead that elastically accommodated sliding is precluded by sufficiently tight

(∼nm) grain-edge interlocking. In marked contrast, the presence of a widely dispersed grain-boundary phase of relatively low viscosity occupying grain-edge tubules seems to be closely correlated with the observation of a broad dissipation peak superimposed upon the high-temperature background. Further experimental work with carefully prepared and characterized materials is needed to assess the generality of this distinction. This disconnect between the existing theory of grain-boundary sliding and the experimental observations of grain-size sensitive viscoelastic relaxation is providing the motivation to revisit the theory in order to clarify the role of sharp/rounded grain edges and the possibility of sliding with concurrent elastic and diffusional accommodation.

Although so far only rarely determined, the grain-size sensitivity of viscoelastic relaxation is potentially diagnostic of the relative contributions of grain-boundary and intragranular mechanisms. For example, the mild grain-size sensitivity of the dissipation and dispersion measured on fine-grained polycrystalline olivine suggests that such grain-boundary processes contribute significantly – but admits the possibility also of significant intragranular contributions.

Dislocation damping is a likely intragranular contributor to seismic wave attenuation especially in the shallower parts of the upper mantle where seismic anisotropy attests to the development of olivine lattice preferred orientation by dislocation creep. The potential of stress-induced migration of (pre-existing) geometrical kinks (Karato, 1998; **Figure 12**) to cause significant relaxation in the seismic frequency band has been demonstrated. However, unequivocal experimental evidence of dislocation damping in upper-mantle materials is limited to the single study of Gueguen *et al.* (1989) that demonstrated a correlation between dissipation and dislocation density. Extensive systematic studies of untreated and variously pre-deformed specimens will be needed to clarify the nature of dislocation relaxation including the role of pinning and the relative contributions of subgrain and subgrain-boundary dislocations. The possibility that both grain-boundary and dislocation relaxation are enhanced by the presence of small concentrations of water-related defects remains to be explored experimentally.

Both dislocation-related and grain-boundary relaxation processes thus have the potential to make substantial contributions to seismic wave dispersion and attenuation. Dislocation relaxation should become progressively more important with increasing grain size for two reasons: (1) prior/ongoing tectonic deformation by dislocation rather than diffusional creep is required to generate an appropriate density of mobile dislocations, and (2) low grain-boundary area per unit volume will diminish the relative importance of grain-boundary relaxation. Thermal activation of the mobility of the defects responsible for the dominant high-temperature background means that solid-state viscoelastic relaxation will become progressively more intense as the relevant solidus is approached. Solid-state relaxation mechanisms may thus account for most of the seismologically observed variation of wave speeds and attenuation.

However, relaxation mechanisms associated with partial melting and phase transformations must also contribute at least locally to viscoelastic relaxation in the mantle. Melt squirt is thought to occur at periods shorter than those of teleseismic wave propagation and accordingly might be partly responsible for reduced wave speeds (but not for the observed attenuation) beneath mid-ocean ridges and in subduction-zone and back-arc environments. Facilitation of elastically accommodated grain-boundary sliding by grain-edge melt tubules, manifest as a broad peak superimposed upon the background dissipation, can produce nearly frequency-independent attenuation across wide ranges of conditions (Faul *et al.*, 2004). In parts of the transition zone, stress-induced variations of the proportions of coexisting phases may result in relaxation of the bulk modulus and associated dissipation of strain energy at tidal and longer periods.

References

Abramowitz M and Stegun IA (1972) *Handbook of Mathematical Functions with Formulas, Graphs, and Mathematical Tables*. New York: Dover Publications.

Aikawa N, Kumazawa M, and Tokonami M (1985) Temperature dependence of intersite distribution of Mg and Fe in olivine and the associated change of lattice parameters. *Physics and Chemistry of Minerals* 12: 1–8.

Anderson OL and Isaak DG (1995) Elastic constants of mantle minerals at high temperature. In: Ahrens TJ (ed.) *AGU Reference Shelf, vol. 2*: *Mineral Physics and Crystallography: A Handbook of Physical Constants*, pp. 64–97. Washington, DC: American Geophysical Union.

Anderson DL and Sammis CG (1970) Partial melting in the upper mantle. *Physics of the Earth and Planetary Interiors* 3: 41–50.

Ashby MF (1972) Boundary defects and atomistic aspects of boundary sliding and diffusional creep. *Surface Science* 31: 498–542.

Barnhoorn A, Jackson I, Fitz Gerald JD, and Aizawa Y (2006) Suppression of elastically accommodated grain-boundary sliding in high-purity MgO. *Journal of the European Ceramic Society* (in press).

Berckhemer H, Kampfmann W, Aulbach E, and Schmeling H (1982) Shear modulus and Q of forsterite and dunite near partial melting from forced oscillation experiments. *Physics of the Earth and Planetary Interiors* 29: 30–41.

Brady JB (1995) Diffusion data for silicate minerals, glasses, and liquids. In: Ahrens TJ (ed.) *AGU Reference Shelf, Vol. 2: Mineral Physics & Crystallography: A Handbook of Physical Constants*, pp. 269–290. Washington, DC: American Geophysical Union.

Brailsford AD (1961) Abrupt-kink model of dislocation motion. *Physical Review* 122: 778–786.

Budiansky B and O'Connell RJ (1980) Bulk dissipation in heterogeneous media. In: Nemat-Nasser S (ed.) *AMD, Vol. 42*: *Solid Earth Geophysics and Geotechnology*, pp. 1–10. New York: ASME.

Budiansky B, Sumner EE, and O'Connell RJ (1983) Bulk thermoelastic attenuation of composite materials. *Journal of Geophysical Research* 88: 10343–10348.

Cooper RF (2003) Seismic wave attenuation: Energy dissipation in viscoelastic crystalline solids. In: Karato S and Wenk H (eds.) *Reviews in Minerology and Geochemistry*: *Plastic Deformation in Minerals and Rocks*, pp. 253–290. Washington DC: Mineralogical Society of America.

Daraktchiev M, Harrison RJ, Mountstevens EH, and Redfern SAT (2006) Effect of transformation twins on the anelastic behavior of polycrystalline Ca_{1-x} Sr_xTiO_3 and $Sr_xBa_{1-x}SnO_3$ perovskite in relation to the seismic properties of Earth's mantle perovskite. *Materials Sciences and Engineering A* 442: 199–203.

Darinskiy BM and Levin YN (1968) Theory of internal friction due to phase transitions. *Physics of Metals and Metallography – USSR* 26(6): 98–105.

Dever DJ (1972) Temperature dependence of the elastic constants in alpha-iron single crystals: Relationship to spin order and diffusion anomalies. *Journal of Applied Physics* 43: 3293–3300.

Durham WB, Goetze C, and Blake B (1977) Plastic flow of oriented single crystals of olivine. Part II: Observations and interpretations of the dislocation structures. *Journal of Geophysical Research* 82: 5755–5770.

Falzone AJ and Stacey FD (1980) Second-order elasticity theory: Explanation for the high Poisson's ratio of the inner core. *Physics of the Earth and Planetary Interiors* 22: 371–377.

Fantozzi G, Esnouf C, Benoit W, and Ritchie IG (1982) Internal friction and microdeformation due to the intrinsic properties of dislocations: The Bordoni relaxation. *Progress in Materials Science* 27: 311–451.

Faul UH, Fitz Gerald JD, and Jackson I (2004) Shear-wave attenuation and dispersion in melt-bearing olivine polycrystals. Part II: Microstructural interpretation and seismological implications. *Journal of Geophysical Research* 109: B06202 (doi:10.1029/2003JB002407).

Faul UH and Jackson I (2005) The seismological signature of temperature and grain size variations in the upper mantle. *Earth and Planetary Science Letters* 234: 119–134.

Faul UH, Toomey DR, and Waff HS (1994) Intergranular basaltic melt is distributed in thin, elongated inclusions. *Geophysical Research Letters* 20(1): 29–32.

Findley WN, Lai JS, and Onaran K (1976) *Creep and Relaxation of Non-Linear Viscoelastic Materials*. Amsterdam: North-Holland.

Friedel G (1964) *Dislocations*. Oxford: Pergamon.

Friedel J, Boulanger C, and Crussard C (1955) Constantes elastiques et frottement interieur de l'aluminium polygonise. *Acta Mettalurgica* 3: 380–391.

Frost HJ and Ashby MF (1982) *Deformation-Mechanism Maps. The Plasticity and Creep of Metals and Ceramics*. Oxford: Pergamon Press.

Gadaud P, Guisolan B, Kulik A, and Schaller R (1990) Apparatus for high-temperature internal friction differential measurements. *Review of Scientific Instruments* 61: 2671–2675.

Getting IC, Dutton SJ, Burnley PC, Karato S, and Spetzler HA (1997) Shear attenuation and dispersion in MgO. *Physics of the Earth and Planetary Interiors* 99: 249–257.

Ghahremani F (1980) Effect of grain boundary sliding on anelasticity of polycrystals. *International Journal of Solids and Structures* 16: 825–845.

Gordon RB (1974) Mechanical relaxation spectrum of crystalline rock containing water. *Journal of Geophysical Research* 79: 2129–2131.

Granato A and Lücke K (1956) Theory of mechanical damping due to dislocations. *Journal of Applied Physics* 27: 583–593.

Gribb TT and Cooper RF (1998a) Low-frequency shear attenuation in polycrystalline olivine: Grain boundary diffusion and the physical significance of the Andrade model for viscoelastic rheology. *Journal of Geophysical Research* 103(B11): 27267–27279.

Gribb TT and Cooper RF (1998b) A high temperature torsion apparatus for the high-resolution characterization of internal friction and creep in refractory metals and ceramics: Application to the seismic-frequency, dynamic response of Earth's upper mantle. *Review of Scientific Instruments* 69: 559–564.

Gribb TT and Cooper RF (2000) The effect of an equilibrated melt phase on the shear creep and attenuation behaviour of polycrystalline olivine. *Geophysical Research Letters* 27(15): 2341–2344.

Gueguen Y, Darot M, Mazot P, and Woirgard J (1989) Q^{-1} of forsterite single crystals. *Physics of the Earth and Planetary Interiors* 55: 254–258.

Gueguen Y and Mercier JM (1973) High attenuation and the low-velocity zone. *Physics of the Earth and Planetary Interiors* 7: 39–46.

Hammond WC and Humphreys ED (2000a) Upper mantle seismic wave attenuation: Effects of realistic partial melt distribution. *Journal of Geophysical Research* 105(B5): 10987–10999.

Hammond WC and Humphreys ED (2000b) Upper mantle seismic wave velocity: Effects of realistic partial melt geometries. *Journal of Geophysical Research* 105(B5): 10975–10986.

Harrison RJ and Redfern SAT (2002) The influence of transformation twins on the seismic-frequency elastic and anelastic properties of perovskite: Dynamical mechanical analysis of single crystal $LaAlO_3$. *Physics of the Earth and Planetary Interiors* 134: 253–272.

Harrison RJ, Redfern SAT, and Salje EKH (2004) Dynamical excitation and anelastic relaxation of ferroelastic domain walls in $LaAlO_3$. *Physical Review B* 69: 144101.

Heinz DL, Jeanloz R, and O'Connell RJ (1982) Bulk attenuation in a polycrystalline Earth. *Journal of Geophysical Research* 87(B9): 7772–7778.

Hensler JH and Cullen GV (1968) Stress, temperature, and strain rate in creep of magnesium oxide. *Journal of the American Ceramic Society* 51: 557–559.

Hudson JA (1981) Wave speeds and attenuation of elastic waves in material containing cracks. *Geophysical Journal of the Royal Astronomical Society* 64: 133–150.

Irifune T and Isshiki M (1998) Iron partitioning in a pyrolite mantle and the nature of the 410-km seismic discontinuity. *Nature* 392: 702–705.

Jackson I (1991) The petrophysical basis for the interpretation of seismological models for the continental lithosphere.

Geological Society of Australia Special Publication 17: 81–114.
Jackson I (1998) Elasticity, composition and temperature of the Earth's lower mantle: A reappraisal. *Geophysical Journal International* 134: 291–311.
Jackson I (2000) Laboratory measurement of seismic wave dispersion and attenuation: Recent progress. In: Karato S, Forte AM, Liebermann RC, Masters G, and Stixrude L (eds.) *Earth's Deep Interior. Mineral Physics and Tomography from the Atomic to the Glocal Scale*, pp. 265–289. Washington, DC: AGU.
Jackson DD and Anderson DL (1970) Physical mechanisms of seismic wave attenuation. *Reviews of Geophysics and Space Physics* 8: 1–63.
Jackson I, Faul UH, Fitz Gerald J, and Morris SJS (2006) Contrasting viscoelastic behaviour of melt-free and melt-bearing olivine: Implications for the nature of grain-boundary sliding. *Materials Science and Engineering A* 442: 170–174.
Jackson I, Faul UH, Fitz Gerald J, and Tan BH (2004) Shear-wave attenuation and dispersion in melt-bearing olivine polycrystals. Part I: Specimen fabrication and mechanical testing. *Journal of Geophysical Research* 109: B06201 (doi:10.1029/2003JB0002406).
Jackson I, Fitz Gerald JD, Faul UH, and Tan BH (2002) Grainsize sensitive seismic wave attenuation in polycrystalline olivine. *Journal of Geophysical Research* 107:B12 2360 (doi:10.1029/2001JB001225).
Jackson I, Fitz Gerald JD, and Kokkonen H (2000) High-temperature viscoelastic relaxation in iron and its implications for the shear modulus and attenuation of the Earth's inner core. *Journal of Geophysical Research* 105: 23605–23634.
Jackson I and Paterson MS (1993) A high-pressure, high-temperature apparatus for studies of seismic wave dispersion and attenuation. *PAGEOPH* 141: 445–466.
Jackson I, Paterson MS, and Fitz Gerald JD (1992) Seismic wave attenuation in Åheim dunite: An experimental study. *Geophysical Journal International* 108: 517–534.
Jackson I, Webb SL, Weston L, and Boness D (2005) Frequency dependence of elastic wave speeds at high-temperature: A direct experimental demonstration. *Physics of the Earth and Planetary Interiors* 148: 85–96.
Jeffreys H (1976) *The Earth: Its Origin, History and Physical Constitution,* 6th edn., 574 pp. Cambridge: University Printing House.
Kamb WB (1959) Theory of preferred crystal orientation developed by crystallization under stress. *Journal of Geology* 67: 153–170.
Kampfmann W and Berckhemer H (1985) High temperature experiments on the elastic and anelastic behaviour of magmatic rocks. *Physics of the Earth and Planetary Interiors* 40: 223–247.
Karato S (1998) A dislocation model of seismic wave attentuation and micro-creep in the Earth: Harold Jeffreys and the rheology of the solid Earth. *PAGEOPH* 153: 239–256.
Karato S and Jung H (1998) Water, partial melting and the origin of the seismic low velocity and high attenuation zone in the upper mantle. *Earth and Planetary Science Letters* 157: 193–207.
Karato S and Spetzler HA (1990) Defect microdynamics in minerals and solid state mechanisms of seismic wave attenuation and velocity dispersion in the mantle. *Reviews of Geophysics* 28: 399–421.
Koehler JS (1952) The influence of dislocations and impurities on the damping and the elastic constants of metal single crystals. In: Shockley W and Hollomon JH (eds.) *Imperfections in Nearly Perfect Crystals*, pp. 197–216. New York: John Wiley & Sons.
Kumazawa M (1969) The elastic constant of polycrystalline rocks and the non-elastic behavior inherent to them. *Journal of Geophysical Research* 74: 5311–5320.
Kê T (1947) Experimental evidence of the viscous behaviour of grain boundaries in metals. *Physical Review* 71(8): 533–546.
Lakki A, Schaller R, Carry C, and Benoit W (1999) High-temperature anelastic and viscoplastic deformation of fine-grained magnesia- and magnesia/yttria-doped alumina. *Journal of the American Ceramic Society* 82(8): 2181–2187.
Leak GM (1961) Grain boundary damping. Part I: Pure iron. *Proceedings of the Physical Society* 78: 1520–1528.
Lu C and Jackson I (2006) Low-frequency seismic properties of thermally cracked and argon saturated granite. *Geophysics* 71: F147–F159.
Mavko GM (1980) Velocity and attenuation in partially molten rocks. *Journal of Geophysical Research* 85: 5173–5189.
Mavko GM and Nur A (1975) Melt squirt in the asthenosphere. *Journal of Geophysical Research* 80: 1444–1448.
Minster JB and Anderson DL (1981) A model of dislocation-controlled rheology for the mantle. *Philosophical Transactions of the Royal Society of London* 299: 319–356.
Morris SJS (2002) Coupling of inerface kinetics and transformation-induced strain during pressure-induced solid-solid phase changes. *Journal of the Mechanics and Physics of Solids* 50: 1363–1396.
Morris SJS and Jackson I (2006) A micromechanical model of attenuation by diffusionally assisted grain-boundary sliding. EOS (Transactions American Geophysical Union) 87(52), Fall Meet. Suppl., Abstract MR21A-0009.
Mosher DR and Raj R (1974) Use of the internal friction technique to measure rates of grain boundary sliding. *Acta Metallurgica* 22: 1469–1474.
Nowick AS and Berry BS (1972) *Anelastic Relaxation in Crystalline Solids*. New York: Academic Press.
O'Connell RJ and Budiansky B (1974) Seismic velocities in dry and saturated cracked solids. *Journal of Geophysical Research* 79: 5412–5426.
O'Connell RJ and Budiansky B (1977) Viscoelastic properties of fluid-saturated cracked solids. *Journal of Geophysical Research* 82: 5719–5735.
Pezzotti G, Kleebe HJ, and Ota K (1998) Grain-boundary viscosity of polycrystalline silicon carbides. *Journal of the American Ceramic Society* 81(12): 3293–3299.
Poirier J-P (1985) *Creep of Crystals. High-Temperature Deformation Processes in Metals, Ceramics and Minerals*. Cambridge UK: Cambridge University Press.
Raj R (1975) Transient behaviour of diffusion-induced creep and creep rupture. *Metallurgical Transactions A* 6A: 1499–1509.
Raj R and Ashby MF (1971) On grain boundary sliding and diffusional creep. *Metallurgical Transactions* 2: 1113–1127.
Schaller R, Fantozzi G, and Gremaud G (2001) (eds.) Mechanical spectroscopy Q^{-1} 2001 with applications to materials science. *Materials Science Forum* 366–368: 683 pp.
Schmeling H (1985) Numerical models on the influence of partial melt on elastic, anelastic and electric properties of rocks. Part I: Elasticity and anelasticity. *Physics of the Earth and Planetary Interiors* 41: 34–57.
Schoeck G (1963) Friccion interna debido a la interaccion entre dislocaciones y atomos solutos. *Acta Metallurgica* 11: 617–622.
Seeger A (1956) On the theory of the low-temperature internal friction peak observed in metals. *Philosophical Magazine* 1: 651–662.
Seeger A (1981) The kink picture of dislocation mobility and dislocation-point-defect interactions. *Journal of Physics IV* 42: 201–228.
Seeger A and Wüthrich C (1976) Dislocation relaxation processes in body-centred cubic metals. *Il Nuovo Cimento* 33: 38–73.

Shearer PM (1999) *Introduction to Seismology*. New York: Cambridge University Press.

Shito A, Karato S, and Park J (2004) Frequency dependence of Q in the Earth's upper mantle inferred from continuous spectra of body waves. *Geophysical Research Letters* 31: L12603.

Shito A, Karato S, Matsukage NK, and Nishihara Y (2006) Toward mapping water content from seismic tomography: Applications to subduction zone upper mantle. In: Jacobsen SD and van der Lee S (eds.) AGU *Monograph V. 168: Earth's Deep Water Cycle*, pp. 225–236. Washington, DC: American Geophysical Union.

Simpson HM and Sosin A (1972) Contribution of defect dragging to dislocation damping. Part I: Theory. *Physical Review B* 5: 1382–1392.

Steinle-Neumann G, Stixrude L, and Cohen RE (2003) Physical properties of iron in the inner core. In: Dehant V, Creager KC, Karato S-I, and Zatman S (eds.) *AGU Geodynamic Series 31*: *Earth's Core, Dynamics, Structure, Rotation*, pp. 137–161. Washington, DC: AGU.

Stixrude L (1997) Structure and sharpness of phase transitions and mantle discontinuities. *Journal of Geophysical Research* 102(B7): 14835–14852.

Stocker RL and Gordon RB (1975) Velocity and internal friction in partial melts. *Journal of Geophysical Research* 79: 2129–2131.

Tan BH, Jackson I, and Fitz Gerald JD (1997) Shear wave dispersion and attenuation in fine-grained synthetic olivine aggregates: Preliminary results. *Geophysical Research Letters* 24(9): 1055–1058.

Tan BH, Jackson I, and Fitz Gerald JD (2001) High-temperature viscoelasticity of fine-grained polycrystalline olivine. *Physics and Chemistry of Minerals* 28: 641–664.

Vaišnys JR (1968) Propagation of acoustic waves through a system undergoing phase transformations. *Journal of Geophysical Research* 73: 7675–7683.

Vočadlo L, Alfè D, Gillan MJ, and Price GD (2003a) The properties of iron under core conditions from first principles calculations. *Physics of the Earth and Planetary Interiors* 140: 101–125.

Vočadlo L, Alfè D, Gillan MJ, Wood IG, Brodholt JP, and Price GD (2003b) Possible thermal and chemical stabilization of body-centred cubic iron in the Earth's core. *Nature* 424: 536–539.

Vočadlo L (2007) *Ab initio* calculations of the elasticity of iron and iron alloys at inner core conditions: Evidence for a partially molten inner core? *Earth and Planetary Science Letters* 254: 227–232.

Walsh JB (1968) Attenuation in partially melted material. *Journal of Geophysical Research* 73: 2209–2216.

Walsh JB (1969) New analysis of attenuation in partially melted rock. *Journal of Geophysical Research* 74: 4333–4337.

Webb S and Jackson I (2003) Anelasticity and microcreep in polycrystalline MgO at high temperature: An exploratory study. *Physics and Chemistry of Minerals* 30: 157–166.

Webb S, Jackson I, and Fitz Gerald JD (1999) Viscoelastic rheology of the titanate perovskites $CaTiO_3$ and $SrTiO_3$ at high temperature. *Physics of the Earth and Planetary Interiors* 115: 259–291.

Weidner DJ and Wang Y (2000) Phase transformations: Implications for mantle structure. In: Karato S (ed.) *Geophysical Monograph Series, vol. 117. Earth's Deep Interior: Mineral Physics and Seismic Tomography From the Atomic to the Global Scale*, pp. 215–235. Washington, DC: American Geophysical Union.

Woirgard J, Mazot P, and Rivière (1981) Programmable system for the measurement of the shear modulus and internal friction, on small specimens at very low frequencies. *Journal of Physics C* 5: 1135–1140.

Xu Y, Zimmerman ME, and Kohlstedt DL (2004) Deformation behaviour of partially molten mantle rocks. In: Karner G (ed.) *MARGINS Theoretical and Experimental Earth Science*, pp. 284–310. New York: Columbia University Press.

Zener C (1941) Theory of the elasticity of polycrystals with viscous grain boundaries. *Physical Review* 60: 906–908.

Zener C (1952) *Elasticity and Anelasticity of Metals*. Chicago, IL: The University of Chicago Press.